Audiomagnetotelluric exploration across Waiʻanae Range, Oʻahu, Hawaiʻi

A final report submitted to the graduate division of the University of Hawaiʻi at Mānoa in partial fulfillment of the requirements for the degree of

MASTER OF SCIENCE

IN

Geology and Geophysics

November 2016

By

Telma Dis Sigurdardottir

Committee:

Garrett Apuzen-Ito
John M. Sinton
Donald M. Thomas

Keywords: Electromagnetics, magnetotellurics, audiomagnetotellurics, geothermal energy, resistivity, hydrology

List of Tables

List of Figures

Contents

Abstract

Geothermal systems are becoming an increasingly important energy source worldwide. With the most expensive electric energy costs in the US (≈30 cents/kWh), it is important to investigate the potential of geothermal resources in Hawaii. Slightly elevated temperature and chloride concentrations, measured in the 1970's at wells in the upper Lualualei Valley, indicate the possibility of a geothermal resource. The objective of this project was to investigate Wai'anae Range, O'ahu, Hawai'i, for resources, including geothermal energy and water, by applying the Audiomagnetotelluric (AMT) method. This method allows us to map electrical resistivity distributions in the subsurface that are affected by fluid chemistry, flow, and temperature. For this study, 22 AMT measurements were recorded in 2015 and 2016 across Wai'anae Range, mainly in Lualualei Valley, Wai'ane Kai, and Schofield Barracks. Preliminary results are presented with apparent resistivity and phase vs. period graphs. The results need further analysis and may require noise filtering, as preliminary results indicate that the measured fields are affected by cultural noise.

1 Introduction

Geothermal exploration is important as the need for harnessing geothermal energy is increasing. As Hawai'i has the most expensive electric energy costs in the US (≈30 cents/kWh), investigating geothermal energy resources is an important enterprise. Geothermal exploration is multidisciplinary and includes approaches of geology, geochemistry, and geophysics (Flóvenz et al., 2012). The AMT and the magnetotellluric (MT) methods are geophysical exploration techniques that can be used to investigate geothermal resource prospects to determine their likely viability (Simpson & Bahr, 2005). The techniques measure the local electric (E) and magnetic (M) fields, which gives information about the electrical resistivity of the subsurface over a range of frequencies. It is important to know the electrical resistivity over a range of frequencies, because it gives us the variation in resistivity with depth, as depth range depends on frequency. Resistivity is related to rock properties (e.g. temperature, presence of weathered minerals, porosity, and hydraulic conductivity) and the fluids present in the rock (e.g. salinity and conductivity). The medium tends to have lower resistivity where the rock is hot or holds high amount of fluid. On the contrary, the medium tends to have high resistivity where the rock is cool or has less fluid. Thus, the potential for geothermal resources is greater in areas with low resistivity. If the subsurface does not consist of hot rock but still yields low resistivity results, that could be an indication of a presence of high fluid content as well as high salinity. This gives important information of a hydrogeologic system, which can help when exploiting the local water source. This project focuses on making measurements of E and M within and around the extinct volcano, Waianae, on Oahu, Hawai'i.

The original goals of the field program were to explore the groundwater distribution and geothermal potential of the Waianae Caldera, and north Mauna Kea, using the AMT and MT methods. That involves determining whether observed resistivities can provide evidence for thermal fluid leakage (warm water migrating through fractures) into the shallow groundwater table and, therefore, indicate the presence of an underlying, geothermal or hydrothermal

system that could provide a source of electrical energy for the island. The possibility of distinguishing between saline water and fresh water was expected, and thereby, insights into the available groundwater resource in the area can be provided. Additionally, this project was originally conducted in order to develop proper practice with the method and the skills required to process and interpret AMT and MT data. By applying two data processing approaches, a 2D and 3D inversion, to the Parker Ranch data collected on Hawaii Island, comparisons can be made between the results, helping estimate similarities between the two approaches.

The purpose of this report, however, is to conduct measurements within the extinct volcano, Wai'anae, on Oahu, and provide a description of how the measurements were recorded. Furthermore, electrical methods, in general, and previous work done on O'ahu are reviewed. The overview of the methods includes description of the basic physics behind the method and the process of going from collected data to the apparent resistivity results is articulated. A review of the geology on O'ahu includes description of geological age, structure, and petrological evolution of the Wai'anae volcano in reference to other volcanoes on the island, providing context for local AMT measurements and related issues of the area. The experimental procedure will be documented in this report along with initial processing of the data, making it ready and accessible for further analysis and inversions.

2 Methods

2.1 Overview of Electromagnetic (EM) methods

There are multiple types of electrical methods used when investigating geothermal and hydrological systems. The methods are either active or passive, depending on the nature of the source (Flóvenz et al., 2012). If the source EMF or electrical potential is produced artificially specifically for the exploration activity, the method is active (Chave & Jones, 2012; Flóvenz et al., 2012). Electrical methods that are active include controlled-source audiomagnetotelluric (CSAMT), time-domain electromagnetic (TDEM), direct current (D.C.) electrical resistivity, and transient electromagnetics (TEM). The TEM method is often used along with the MT method to jointly invert for the data in order to correct for the "static shift", which is caused by heterogenity around the electrodes (Flóvenz et al., 2012). Direct current (D.C.) methods include very low frequency (VLF) induction studies, vertical electrical resistivity Schlumberger soundings (VES), Schlumberger, and equatorial dipole-dipole electrode methods.

Passive EM methods record naturally occurring electromagnetic signals. The AMT and MT techniques are reliable and cost effective methods for measuring the local electric and magnetic fields and using that information for infering how electrical resistivity varies with depth in the ground (Pierce & Thomas, 2009). AMT/MT methods can detect structures on a wide range of scales, from about 1 km to many tens of km, which is a great advantage in geothermal exploration (Key et al., 2013). MT method uses lower frequencies than AMT and therefore achieves greater exploration depths, sometimes tens to hundreds of kilometers (Flóvenz et al., 2012). AMT uses higher frequencies and therefore produces higher resolution to much lower depths, often down to only about one kilometer (Stratagem, 2007).

2.2 Summary of the physical processes of the AMT and MT methods

Here, I provide a broad summary of how the MT and AMT methods work. The electromagnetic field signals for the methods originate from two different sources in the magnetosphere (Chave & Jones, 2012). The first source originates from the interaction of the time-varying solar wind with Earth's magnetic field within the magnetosphere (Naidu, 2012; Constable, 2016). These are low frequency (lower than 1 Hz) signals, which are used for deeply penetrating MT surveys. The second source originates from thunderstorm activity within the waveguide between the ionosphere and Earth's surface (Naidu, 2012; Constable, 2016). These are high frequency signals (greater than 1 Hz) and span the interval used for shallow AMT measurements.

The horizontal components of the magnetic waves, from sources above, are measured by the magnetic sensors of the receiver on the surface. This magnetic signal is considered to be the measured "source" signal. The magnetic energy travels into the subsurface where it induces electrical currents. The induced electrical currents travels through the Earth and produces voltage differences on the surface. These voltage differences are detected by electrodes and are the measured Earth "response" signal. The relationship between the incident magnetic source field vector ($\mathbf{M}$) and the induced electrical response vector ($\mathbf{E}$) is the impedance tensor ($\underline{Z}$), and it reflects the resistivity of the rock through which the E and M fields traveled.

The depths to which the energy propagates depends on two factors: resistivity itself and the frequency of the incident energy. Highly resistive material in the subsurface, allows electromagnetic energy to travel deeper into the Earth; in contrast, material that has low resistivity causes electromagnetic energy to decay faster, thus penetrating to shallower depths (Chave & Jones, 2012). In addition, longer period energy tends to propagate deeper into the earth compared to shorter period energy. The combined effects of resistivity and period on the depth of penetration can be described by the "skin-depth" (δ) approximation (see eq. 1) (Cagniard, 1953; Chave & Jones, 2012),

$$\delta = 503\sqrt{\rho T}, \tag{1}$$

where T is period in seconds and ρ is resistivity in Ohm-m. This equation provides a "rule-of-thumb" measure of the depth of energy penetration. Making measurements using a range of periods can provide information about how deep the electromagnetic waves propagate. The tensorial relationship between M and E is used to compute the "apparent resistivity" ; measuring apparent resistivity over a range of periods thus provides information about variations in resistivity with depth. Measuring apparent resistivity at different geographic locations provide information about variations in resistivity with both depth and along a measured profile or grid. Thus AMT and MT method can be used to construct 2-D and 3-D resistivity models within the subsurface.

2.3 First principals and relating measured E and M fields to apparent resistivity

The Maxwell's equations describe the behavior of electromagnetic fields (Simpson & Bahr, 2005) and are used here to formally relate the measured magnetic field (source) and the measured electrical field (response).

Two of Maxwell's equations are
Faraday's law

$$\nabla \times \mathbf{E} = -\mu \frac{\partial \mathbf{H}}{\partial t} \tag{2}$$

and Ampére's law

$$\nabla \times \mathbf{H} = \sigma \mathbf{E} + \epsilon \frac{\partial \mathbf{E}}{\partial t}. \tag{3}$$

- $\mathbf{E}$ is the electric field in volts per meter (Vm^{-1})
- $\mathbf{H}$ is the magnetic intensity in Ampere per meter (Am^{-1})
- μ is the magnetic permeability.
- ϵ is the electrical permittivity.
- σ is the conductivity
- $\nabla\times$ and $\nabla\cdot$ are the calculus expressions curl and div.

A key approximation made is that the EM energy from the ionosphere propagates down to the Earth as a plane wave (Tikhonov, 1950). A vertically incident plane wave allows for Eq. 2 and 3 to be greatly simplified by making partial derivatives with respect to the horizontal directions zero

$$\frac{\partial}{\partial x} = \frac{\partial}{\partial y} = 0. \tag{4}$$

This gives Faraday's and Ampére's laws only in terms of derivatives with respect to z and t. The next simplifying step is to convert the time series of the two horizontal components of both $\mathbf{E}$ and $\mathbf{H}$ fields into the frequency domain using Fourier transforms. This is convenient and powerful in this application, because it removes the time-derivatives in the equations. The following equations express Fourier transforms for a variable and the time derivatives of that variable

$$\mathcal{F}\{x(t)\} = \hat{x}(\omega) = \int_{-\infty}^{\infty} x(t) e^{-i\omega t} dt, \tag{5}$$

$$\mathcal{F}\left\{x^{(n)}(t)\right\} = (i\omega)^n \hat{x}(\omega) = (i\omega)^n \int_{-\infty}^{\infty} x(t) e^{-i\omega t} dt, \tag{6}$$

where $\mathcal{F}$ is the symbol for Fourier transform operator, $x(t)$ is any time dependent variable (in the time domain), $\hat{x}(\omega)$ is the corresponding frequency dependent variable (in the Fourier or frequency domain), $x^{(n)}(t)$ is the n^{th} time derivative of $x(t)$, and ω is the angular frequency.

What remains are the two equations expressed as ordinary differential equations involving vertical derivatives of the Fourier transform fields. Combining and solving the two equations and applying some algebraic substitutions (See Appendix A) yields the following solutions for the Fourier transforms of **E** and **H**.

$$\hat{\mathbf{E}}(\omega) = \hat{\mathbf{E}}_0 e^{i\omega t - kz} \tag{7}$$

$$\hat{\mathbf{H}}(\omega) = \hat{\mathbf{H}}_0 e^{i\omega t - kz} \tag{8}$$

Here $\hat{\mathbf{E}}(\omega)$ is the Fourier transform of the electric field vector and $\hat{\mathbf{H}}(\omega)$ is the Fourier transform of the magnetic intensity vector, $\hat{\mathbf{E}}_\mathbf{0}$ and $\hat{\mathbf{H}}_\mathbf{0}$ are the initial amplitudes at the surface (z=t=0), and k is the wave number (Vozoff, 1972; Gamble et al., 1979; Simpson & Bahr, 2005).

The transformed functions express the relationship between the electric and magnetic fields (equations 7 and 8), and are given by (Gamble et al., 1979; Vozoff, 1990; Simpson & Bahr, 2005):

$$\hat{E}_x(\omega) = \hat{Z}_{xx}(\omega)\hat{H}_x(\omega) + \hat{Z}_{xy}(\omega)\hat{H}_y(\omega) \tag{9}$$

$$\hat{E}_y(\omega) = \hat{Z}_{yx}(\omega)\hat{H}_x(\omega) + \hat{Z}_{yy}(\omega)\hat{H}_y(\omega) \tag{10}$$

which can be written as:

$$\begin{pmatrix} \hat{E}_x \\ \hat{E}_y \end{pmatrix} = \begin{pmatrix} \hat{Z}_{xx} & \hat{Z}_{xy} \\ \hat{Z}_{yx} & \hat{Z}_{yy} \end{pmatrix} \begin{pmatrix} \hat{H}_x \\ \hat{H}_y \end{pmatrix} \tag{11}$$

or $\hat{\mathbf{E}} = \underline{\hat{Z}}\hat{\mathbf{H}}$, where $\hat{\mathbf{E}}$ is related to $\hat{\mathbf{H}}$ through the impedance tensor, $\underline{\hat{Z}}$.

From the impedance tensor (eq. 11) we can obtain the resistivity and phase with the following

$$\rho_{ij} = \frac{1}{\omega\mu_0}|\hat{Z}_{ij}|^2 = \frac{0.2}{f}|\hat{Z}_{ij}|^2, \tag{12}$$

$$\phi_{ij} = tan^{-1}\left(\frac{Im(\hat{Z}_{ij})}{Re(\hat{Z}_{ij})}\right). \tag{13}$$

Here $\hat{Z}_{ij}$ is the scalar surface impedance and relates simply to the fields through

$$\hat{Z}_{ij} = \frac{\hat{E}_i}{\hat{H}_j}, \tag{14}$$

where $i = x, y$ and $j = x, y$, ρ_{ij} is the apparent resistivity, and ϕ_{ij} is the phase.

3 Background and previous work

3.1 Prior applications of electrical methods in Hawaii

In the past decades, resistivity techniques have been applied in Hawaii, as well as in other volcanic areas around the world. Here, I summarize some applications for providing insight into elevation of transition zones (where fresh water meets saline water), saturation zones, groundwater setting, and resistivity anomalies linked to heat sources of volcanic systems.

Resistivity techniques have been applied to gain insights about the groundwater resources in the Hawaiian Islands. Zohdy and Jackson (1969) conducted surveys on Oʻahu and Hawaiʻi (Big Island) in order to investigate the hydrogeologic setting, specifically to locate freshwater aquifers. Both Schlumberger and the bipole-dipole electrode configurations were used (Zohdy & Jackson, 1969). Zohdy and Jackson (1969) concluded that the groundwater seems to be impounded within a dike at about 900 m depth, within Island of Hawaiʻi, near Pohakuloa and Humuula. Lepley and Adams (1969) used the AMT method to investigate the resistivity structure on Hawaiʻi Island, in order to obtain a clearer idea of the sea-water interface depth and the dike system. They found a sharp contrast in resistivity between 100 m and a few km depth, which they state could be caused by either different rock materials from Mauna Kea and Mauna Loa or the difference in depression of the saline/freshwater - saltwater interface from north to south (W. M. Adams et al., 1969). Pierce and Thomas (2009) used MT and AMT soundings to search for potable water in the Saddle Region of Hawaiʻi Island. They found the groundwater level to be higher, at about 1,000 m above sea level, than previous models had suggested . They emphasize that their results cannot confirm whether the water resource exists, however, their findings can help eliminate areas where exploiting water would not be successful.

A groundwater investigation such as those above was conducted on different islands of Hawaiʻi. An example of that is a survey that was conducted on Maui by the Hawaii Institute of Geophysics Direct Heat Regional Assessment Program (Mattice, 1981). The main conclusion was that the freshwater lens is thin and close to the coastline, and the lowest resistivities were found at Ukumehame canyon on West Maui (Mattice, 1981).

Resistivity surveys have also been performed to investigate geothermal resources. A time-domain electromagnetic (TDEM) sounding survey was conducted on the East Rift of Kīlauea Volcano, Hawaiʻi, in 1974 (Kauahikaua, 1981). Conductivities were found to increase with depth. At depths greater than 1 km a zone of high-temperature fluids is indicated beneath the geothermal area of the East Rift, south of the rift, and east of Pahoa (Kauahikaua, 1981). Zablocki (1976) mapped thermal anomalies on Kīlauea using the self-potential, one of the most useful methods to identify thermal anomalies in geothermal and volcanic zones. The SP results confirm the depth to a conductive zone of 250 m (Zablocki, 1976a). They concluded that this method can be successfully applied to investigate active volcanoes, such as Kīlauea, for magma or hot rock (Zablocki, 1976a). Jackson and Sako (1983) applied the SP technique on Kīlauea and Hualālai volcanoes. The first finding they made was that topographic adjustments should be applied to all of the data (Jackson & Sako, 1983). Their second result was that the depth to a high-level dike-impounded water beneath the summit of Hualālai is at about 500 m deep (Jackson & Sako, 1983). A self-potential survey was conducted in the Puhimau thermal area, on the east rift of Kīlauea, Hawaiʻi

(Anderson, 1984), along with VLF tilt angle measurements, VLF resistivity technique, DC Schlumberger resistivity soundings. Anderson (1984) found a magma body at the depth of only 280 m, on their northwest-southwest profile, which is located near the Puhimau pit-crater and thermal area; those results were obtained with the DC Schlumberger technique. Puhimau thermal area is warm to touch, therefore the location of the magma body of only 280 m may be reasonable. In 1984, a CSAMT survey was performed by Sandia National Laboratories (Sandia) at the Puhimau area (Bartel & Jacobson, 1987). The purpose of this was to determine the depth of any molten magma or hot water zones in the geothermal area of Puhimau (Bartel & Jacobson, 1987). Bartel and Jackson (1987) found a geologic feature that could be a dike at 200 m depth, connected to a conducting basal layer at 350 m depth.

To study the nature of magmatic systems electrical and magnetic studies were performed by Zablocki (1976) to investigate hot areas; such as Kīlauea Iki lavas. This survey was expected to give good results for determining where the edges of the melt area (Zablocki, 1976b). The apparent Curie temperature of the Kīlauea Iki lava was found to be 540^{o}C through these studies, and that is the most significant result. Jackson and others (1985) used controlled source electromagnetic (CSEM) methods near the summit of Kīlauea. The purpose of this survey was to study volcanic processes and map intrusions at depth (Jackson et al., 1985). Jackson and others (1985) conclude that CSEM can be used to detect magmatic events that seismic monitors or other geodetic methods cannot, and that intrusive events associated with shallow magmatic emplacement are detectable by CSEM.

Many studies have successfully used electrical methods to locate resistivity anomalies, that reveal information about groundwater reservoirs, geothermal systems, and magmatic setting within volcanic areas in Hawai‘i. The study areas are commonly geologically mapped before applying the electrical methods, therefore, allowing the scientists to pick areas, which would be most prominent to encounter useful sources. As for this project, the area within Wai‘anae Caldera is chosen for conducting an AMT survey, as that would be the most likely area to contain heat, according to geologic mapping made in the past 50 years.

3.2 Geology of Wai‘anae Range, O‘ahu, Hawai‘i

Wai‘anae Volcano is an extinct volcano and is located on west O‘ahu Island, in the Hawaiian Archipelago. It is one of three volcanoes that built O‘ahu. The Ko‘olau Volcanics (age <3 Ma), younger than Wai‘anae, is located on East O‘ahu (Stearns & Vaksvik, 1935) and Ka‘ena Volcano with the age between 3.4-5 Ma, which is older than Wai‘anae lies just offshore of O‘ahu to the northwest (Sinton et al., 2014). The geological age of Wai‘anae is between 2.9 to 3.93 Ma (Presley et al., 1997; Guillou et al., 2000), which partly spans both Gilbert (reversed polarity) and Gauss (normal polarity) Chrons. The age estimate derives from potassium-argon radiometric data of volcanic rocks (McDougall, 1964; Funkhouser et al., 1968; Doell & Dalrymple, 1973; Presley et al., 1997; Laj et al., 1999; Guillou et al., 2000). Along with radiometry, paleomagnetism can give valuable information about the age and stratigraphy (Guillou et al., 2000; Sherrod et al., 2007). The radiometric ages for Wai‘anae Volcanics are displayed in Figure 1. During Wai‘anae's volcanic activity, magnetic polarity reversal occurred twice within Gauss, including Ka‘ena and Mammoth reversed-polarity subchrons within the Gauss normal Chron (Guillou et al., 2000; Sherrod et al., 2007).

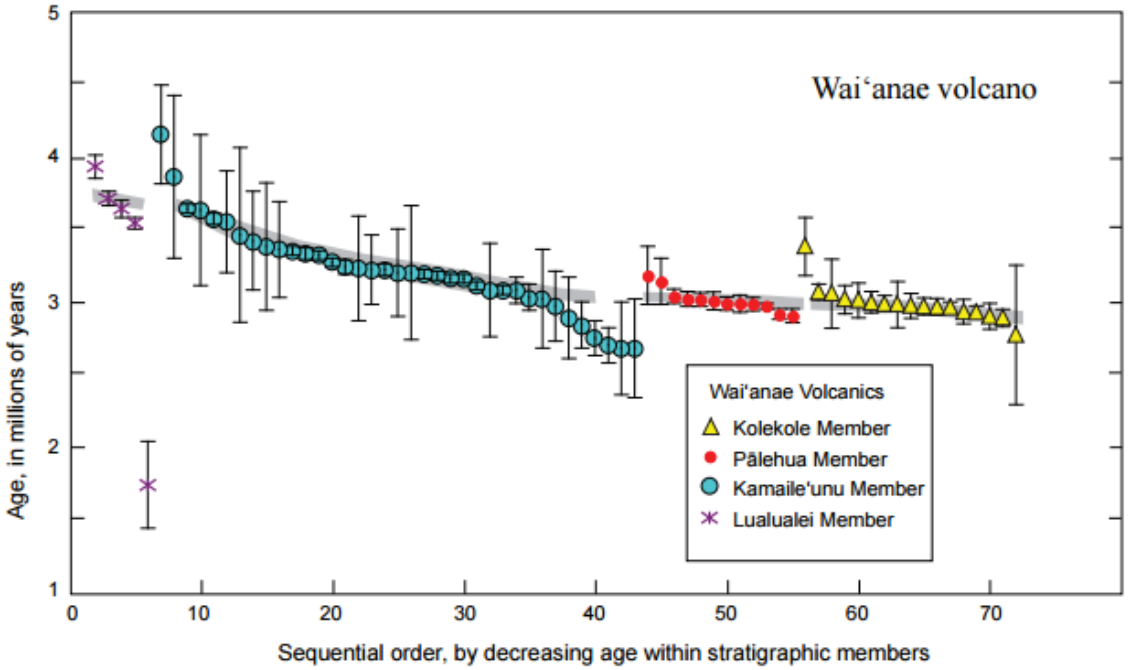

Figure 1: Wai‘anae volcanic members ages, obtained from radiometric ages (McDougall, 1964; Doell & Dalrymple, 1973; Presley et al., 1997; Laj et al., 1999; Guillou et al., 2000). Gray areas indicate the most likely range of ages (Sherrod et al., 2007).

The Wai‘anae Volcanics (see Fig. 2 for a visual geological explanation) are divided into four members: Lualualei, Kamaile‘unu, Pālehua, and Kolekole Members (Presley et al., 1997). The members subsequently represent the evolution of the Wai‘anae Volcano. Typically, the evolution of a Hawaiian volcano occurs in up to four main stages: preshield, shield, postshield, and rejuvenated (Clague & Sherrod, 2014). The stages are distinguished based on the rate of eruption, eruptive style, development, and magma composition (Wolfe et al., 1997). The Lualualei member consists of tholeiitic basalt shield-building lavas, which have reversed polarity magnetization, and is the oldest of the exposed lavas. Lualualei member's ages are displayed among the other three members on Figure 1, with its ages from 3.55 to 3.93 Ma (Guillou et al., 2000). The Kamaile‘unu member is a late-shield phase, which occurred between 3.55 to 3.06 Ma during the Gauss normal-polarity Chron lasting until early Ka‘ena subchron (Presley et al., 1997). The eruptions during this phase occurred within Wai‘anae caldera, which got filled with lavas at the time (Sherrod et al., 2007). Wai‘anae's eruptive activity started to decline during the Kamaile'unu member, while the magmatic system subsided as the volcano migrated away from the Hawaiian hot spot (Presley et al., 1997). Alkalic lavas are more abundant (Presley et al., 1997) during Kamaile‘unu, because of lower degree mantle melting, which occurs in cooler magmatic systems. Pālehua member is a postshield phase of hawaiite to mugearite volcanism and is younger than 3.06 Ma old (Presley et al., 1997), mostly with normal magnetic polarity, but with a few older reversed samples from the Ka‘ena subchron. The Kolekole member is a post-erosional phase of basaltic postshield activity and is the youngest member of the Wai‘anae volcanic series, with the age of 2.98 Ma and normal polarity during Gauss Chron (Presley et al., 1997).

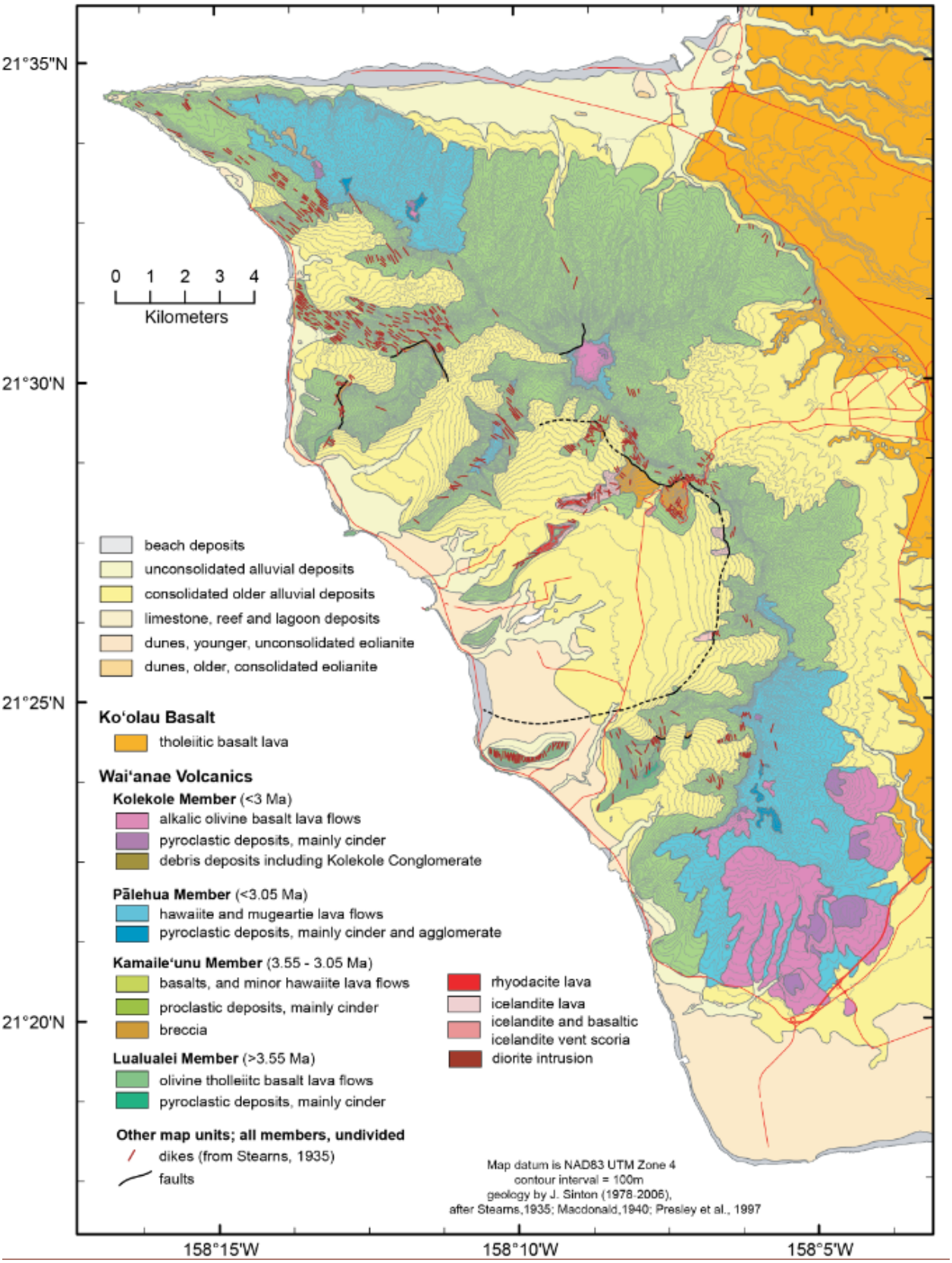

Figure 2: Geology map of West Oahu (Compiled by Sinton, data from (Sherrod et al., 2007)).

Waiʻanae volcano is located on the shoreline, as opposed to younger volcanoes, which are located further inland. The reason for this location in reference to younger volcanoes, is that Waiʻanae Volcano has drifted away from the hot spot and had a landslide event about 3 Ma. The landslide occurred before Kolekole Member events (Presley et al., 1997) and caused major erosion, leaving the evidence of what is called the Waiʻanae Slump (Presley et al., 1997). Waiʻanae Slump (Moore et al., 1989) is located off shore west of the volcano. Waiʻanae's western slope has been eroded and therefore, revealing its internal structure.

The landslide event has an impact on Waiʻanae's geothermal potential, as subsiding magmatic system means that the system is cooling. There are possibly four rift zones (see Figure 3); on which the eruptions occurred (Stearns & Vaksvik, 1935; Zbinden & Sinton, 1988; Sinton et al., 2014). Many dikes mark these rift zones in surface exposures and they are parallel to the rift zones (Zbinden & Sinton, 1988), which indicates the direction of weakness within the crust. The caldera boundary is roughly estimated and presented in Figure 2. Figure 2 shows that the caldera has a diameter of about 8 km and its center is located between Waiʻanae Valley and Lualualei Valley (Sinton, 1986; Zbinden & Sinton, 1988; van der Zander et al., 2010; Presley et al., 1997). Those two valleys are separated by the ridge Paheʻeheʻe and Mauna Kūwale, which consists of icelandite and rhyodacite (van der Zander et al., 2010). The rhyodacite is about 3.3 million years old (Guillou et al., 2000) with silica content of approximately 66 wt % (van der Zander et al., 2010) and is shown in red shades on Figure 2.

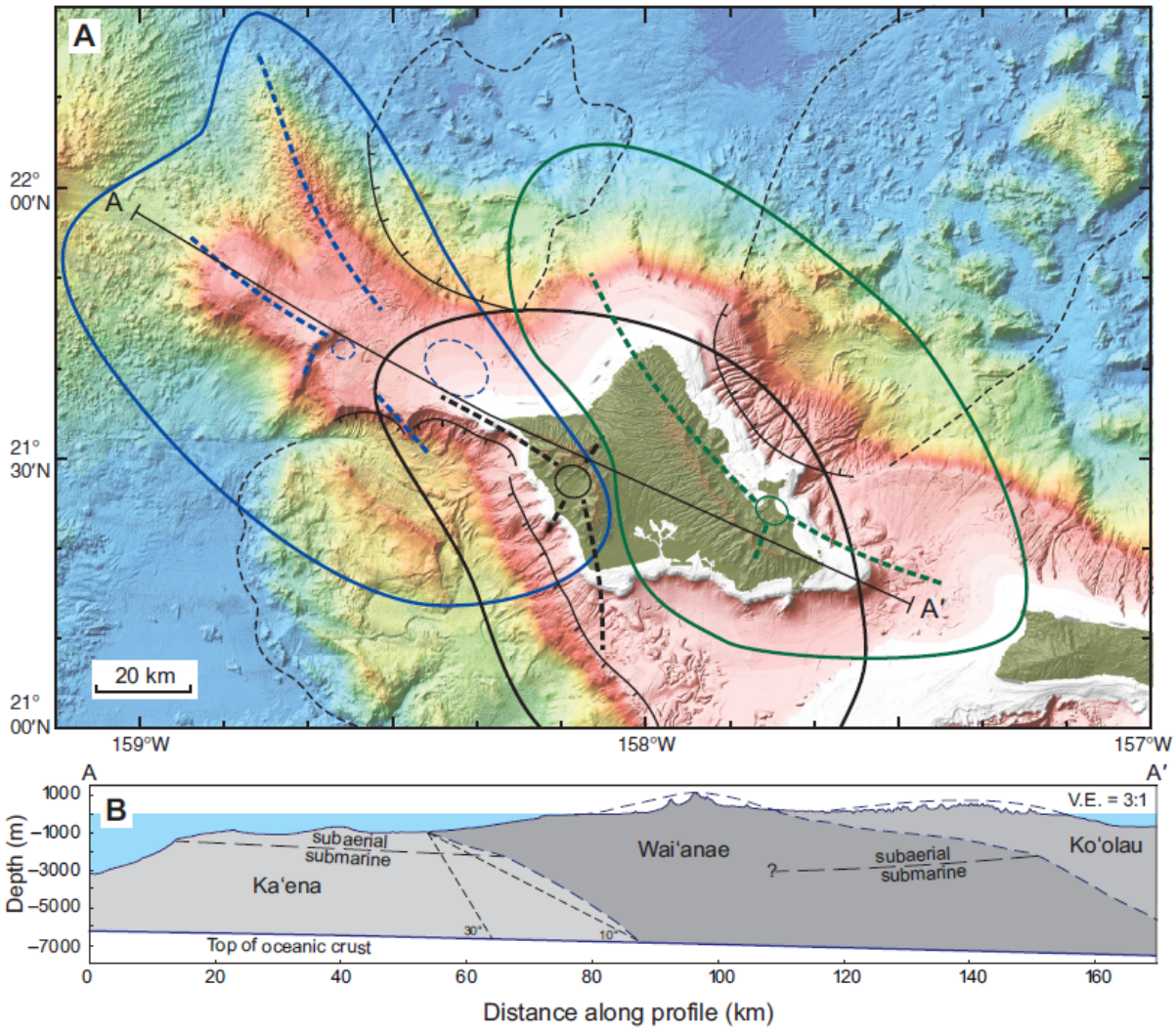

Figure 3: Oahu rift zones are presented with dotted lines and the caldera region is presented with a circle on the west part of O‘ahu (Sinton et al., 2014).

The studies performed during the last $\sim$ 40 years include, geochemistry, radiometry, and paleomagnetism and provide a viable background for any geophysical studies in the area. Composition, structure, and the geologic age of a volcano, such as for Wai‘anae Volcano, are useful information for investigating geothermal systems, because it provides a better understanding for interpreting geophysical data. Geophysical techniques such as the electrical method that was used for this project (AMT), detect different results for different geologic features. We are interested in the areas within the caldera and the rift zones around the caldera, where the dikes are concentrated; because those are magmatic centers and are most likely to contain heat. Rift zones are permeable parallel to the dike swarms, which is another reason it could contain heat. The structure of the Wai‘anae Volcano is important, as dike orientation represent rift zones and tells us where the system weaknesses are. Depending on the distance from the magma body, the potential of encountering a geothermal reservoir is greater with shallower depths. The petrological evolution gives insight into magma melting

processes, which depend on the distance away from the hot spot. Waiʻanae Volcano possibly has heat left within it, however, the reason for investigating this area, is to estimate how much of it there is and where and how deep it is located. Waiʻanae Range is an interesting area for geothermal assessment, because it is a volcano, of which previous studies in the 1970's indicate a potential for geothermal area (Thomas et al., 1979). Some evidence of heat left in the volcano does exist (Thomas et al., 1979), such as elevated groundwater temperatures, moderate Cl/Mg ratios, and low resistivity results from preliminary resistivity measurements within Lualualei Valley.

3.2.1 Prior Geophysical Work on Waiʻanae

Resistivity work was conducted on Oahu using the dipole mapping technique in the 1970's (Grose & Keller, 1975). Geophysical exploration previously conducted on Oahu includes aeromagnetic surveys (Malahoff & Woollard, 1966), gravity surveys (Strange et al., 1965), and seismic investigations (W. Adams & Furumoto, 1965). Geophysical exploration done specifically in Lualualei Valley are self-potential, rotating quadripole resistivity, and shallow soil temperature surveys. What those limited geophysical surveys detected is low resistivity values within the Waiʻanae Caldera, which coincided with slightly elevated subsurface groundwater temperatures (to about 25°C) at 1 m depth. Previous groundwater chemistry work done in the Lualualei area includes silica concentrations and Cl/Mg ratios (Thomas et al., 1979). The variations in silica concentration did not give insight of whether thermal activity was present, however, Cl/Mg ion anomalies are moderate (ratios with the values of 12-15) in the area (Thomas et al., 1979). Additionally, groundwater temperatures that are slightly elevated within the caldera (see caldera region in Fig. 3), measured in the local wells, indicate the potential for a geothermal resource in this area.

4 AMT Data acquisition and processing

Each site is precisely located and set up with electrical and magnetic sensors oriented orthogonally to each other (Stratagem, 2007). Figure 4 shows a typical setup of an AMT site, consisting of four components: N-S- and E-W electric dipoles, and N-S- and E-W magnetic coils. Electric dipoles have one electrode on each end, with a total of four electrodes. An electrode is a T-shaped stainless steel stake that is about 50 cm long with a diameter of about 2 cm. The electrode spikes are inserted into the ground using a hammer on all ends. An electric cable is attached to the electrodes, which lies on the surface and is connected to the analog front end (AFE), located in the center of the site setup.

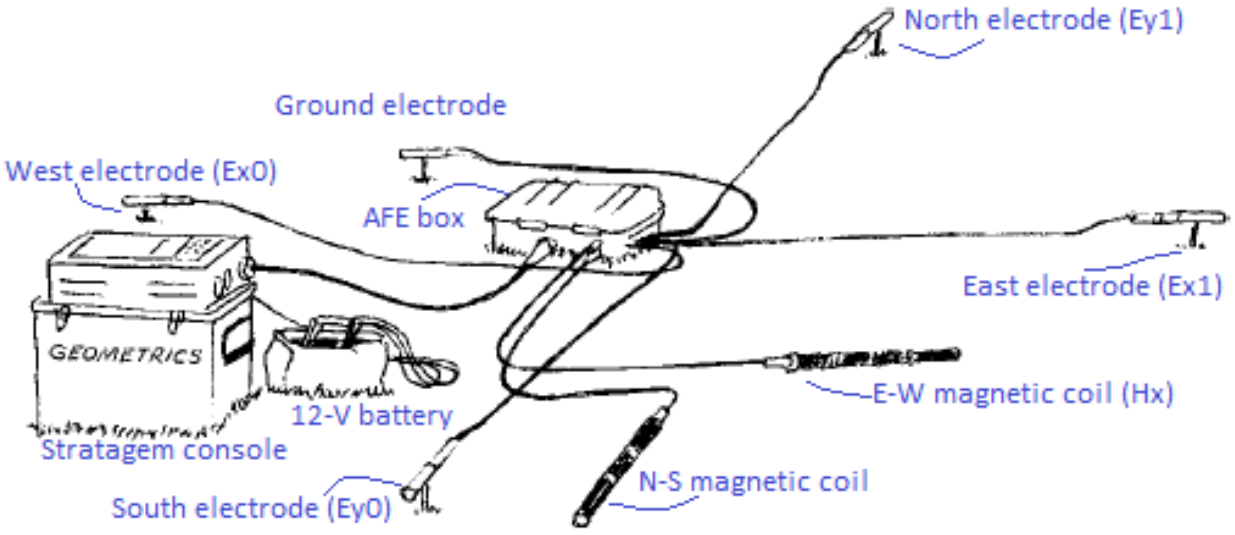

Figure 4: A layout of the Stratagem receiver (Stratagem, 2007). The console is labelled with GEOMETRICS, and it is connected to a 12-V battery, a keyboard (missing from the sketch), and the AFE box, located in the middle of the setup in the figure. Two magnetic sensors, four electrodes, and a fifth electrode (used to ground the measurement) are all connected to the AFE.

Both magnetic coils are connected to the AFE box in a similar way as the electrodes. The coils are positioned a few meters away from the center. They are placed carefully, levelled, and precisely oriented in N-S and E-W directions. When the sensors are placed, it is important to use a compass at least 0.5 m away from the coil to prevent distortion in the magnetic field. Placing soil over the coil will help to keep it in the right orientation and level, and reduces any mechanical disturbance of the coil that can produce electrical noise in the coil.

The AFE (see Figure 5) is connected with a serial cable to the Stratagem console, which is shown in Figure 6, labelled with GEOMETRICS. The console is located at least 5 meters away from the AFE and connected to both a 12-V battery and a keyboard. Once everything is connected to the console and gains for all frequency bands have been set, data acquisition can start. Data acquisition usually takes about half an hour for all frequency bands, which are: low frequency band (10-1 kHz), mid frequency band (500-3kHz), and high frequency band (750-92kHz). For synchronized data acquisition the Stratagem transmitter is used along with the high frequency band segments. Such a transmitter is shown in Figure 6. Synchronization must start within 3 seconds of the start of acquisition for the high frequency band.

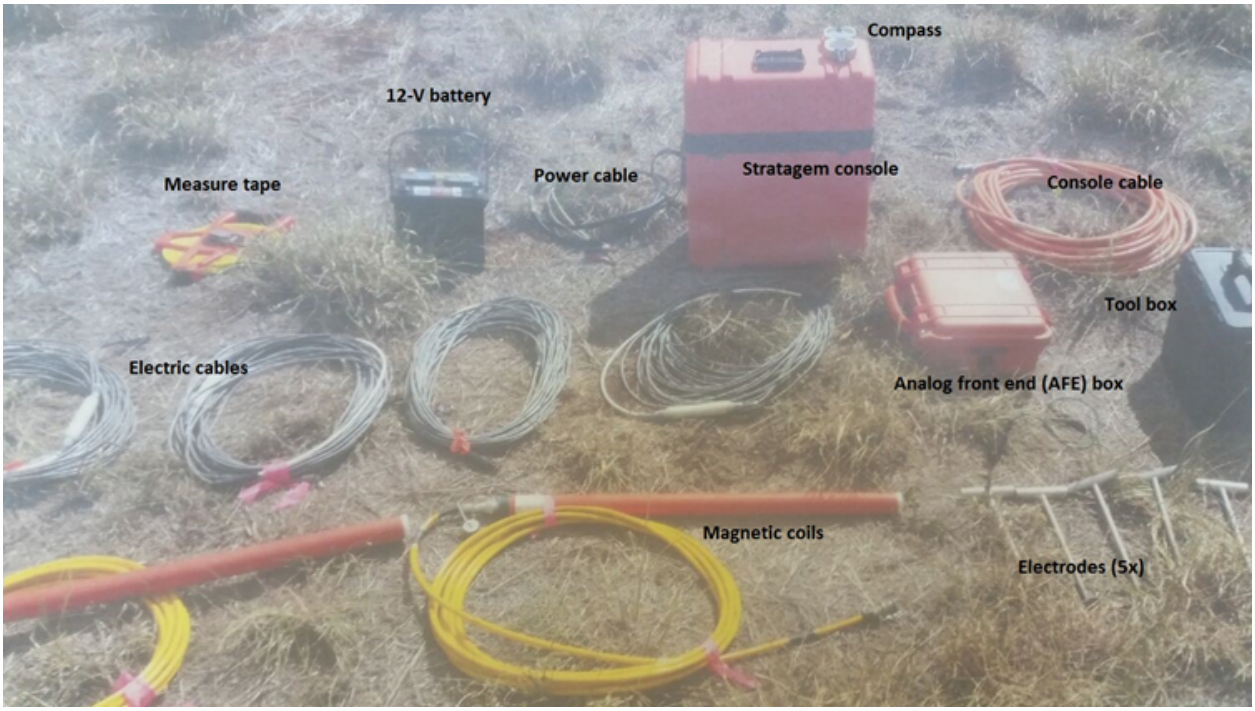

Figure 5: AMT equipment used for measurements.

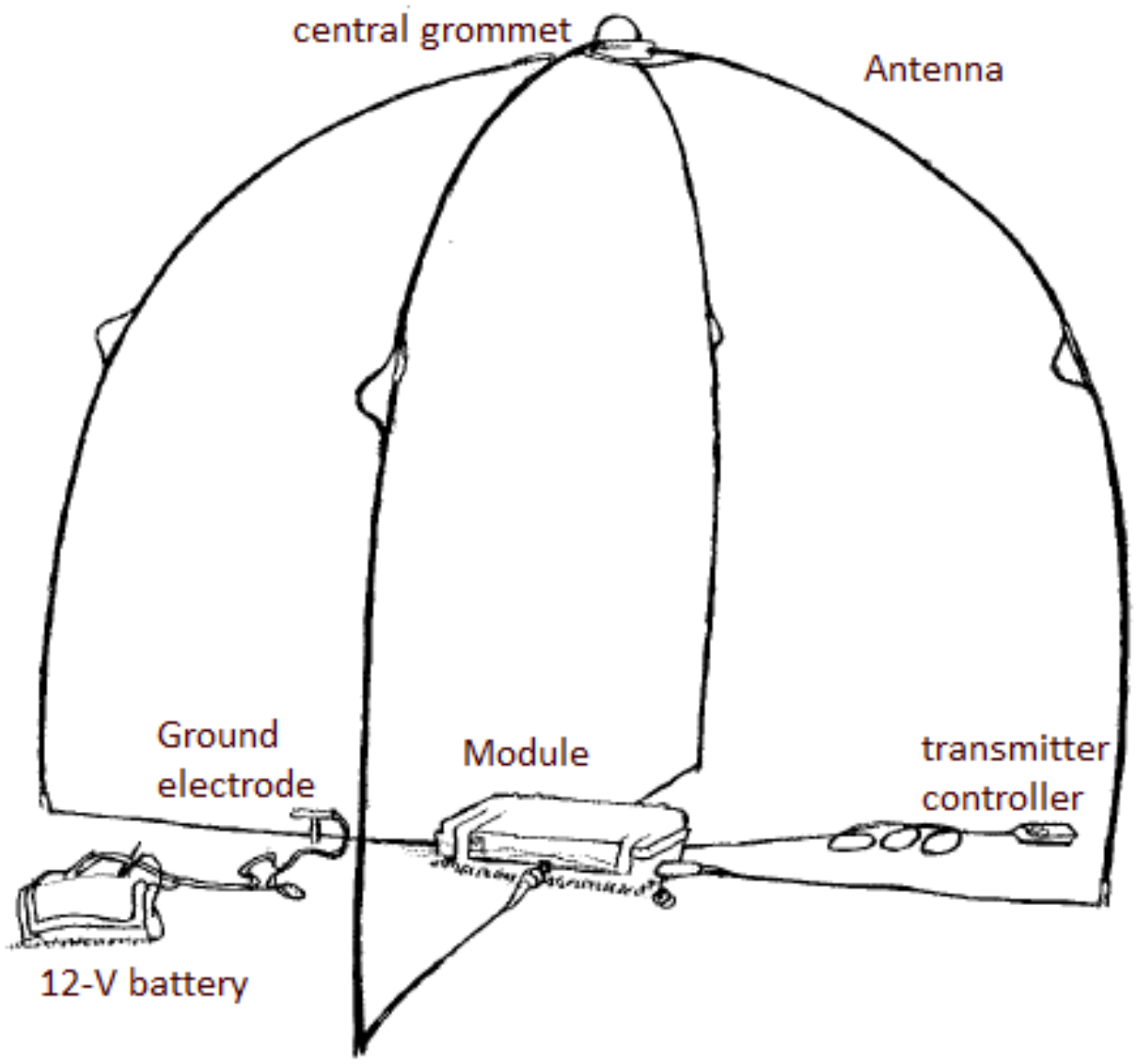

Figure 6: Setup of the Stratagem transmitter (Stratagem, 2007). The transmitter consists of an antenna, a box, a button to start the transmitting signal, and a ground electrode.

Location of the transmitter depends on the location of the measurement. The mesurement site must be placed in the transmitter's far field, which is three times the distance of the skin depth at the measuring site. Since the skin depth is dependent on conductivity or resistivity, the distance between the transmitter and the site increases with the resistivity (Stratagem, 2007).

Once data acquisition is completed and we have the magnetic and electric field time series, data processing can begin. Data processing of AMT data includes: (1) using the Stratagem Imagem software (imagem) to modify, using fast Fourier transform function (FFT) to convert time series from time domain to frequency domain, and obtaining the impedance estimates, plotting the tensor apparent resistivity and phase against log10Period; (2) using

the WinGLink software for inversion in one and two dimensions (1D, 2D), modeling, and interpretations; (3) performing 3D analysis, using ModEM (Kelbert & Egbert, 2011; Egbert & Kelbert, 2012; Kelbert et al., 2014); and (4) performing 3D analysis, using WSINV3DMT (Siripunvaraporn, 2012).

4.1 Imagem software, FFT, and other calculations

The Stratagem Imagem software automatically converts time series to spectral data, calculating the cross-power and impedance results. Time series convert to FFT and FFT to raw spectra (Stratagem, 2007). Then conversion of spectral data to impedance data occurs. Impedance files include scalar apparent resistivity and phase values for E_xH_y and E_yH_x.

Resistivity and phase values are obtained from the impedance files automatically generated by the Stratagem instrument (Stratagem, 2007). Each site has its own impedance file, time series file, and cross power file. The impedance file is a result of impedance calculated from cross power and time series file; it includes frequency, coherency between orthogonal components of electric field and magnetic field, scalar apparent resistivity and phase, and real and imaginary parts of the impedance estimates. See Table 1 for elements of the impedance file.

Table 1: Elements of an impedance file (Stratagem, 2007).

Column	Line 1	Line 2
1	frequency in Hz	re Zxx/$\sqrt{(\omega\mu_0)}$
2	ExHy coherency	im Zxx/$\sqrt{(\omega\mu_0)}$
3	ExHy scalar apparent resistivity	re Zxy/$\sqrt{(\omega\mu_0)}$
4	ExHy scalar phase	im Zxy/$\sqrt{(\omega\mu_0)}$
5	EyHz coherency	re Zyx/$\sqrt{(\omega\mu_0)}$
6	EyHx scalar apparent resistivity	im Zyx/$\sqrt{(\omega\mu_0)}$
7	EyHx scalar phase	re Zyy/$\sqrt{(\omega\mu_0)}$
8	<blank>	im Zyy/$\sqrt{(\omega\mu_0)}$

Conversion from time domain to frequency domain involves Fourier transform (Simpson & Bahr, 2005). This transform function is a ratio of the input processes and output processes, with the Earth's time varying magnetic field as the input process and the time varying electric field as the output process. The choice of a statistical method is based on the noise level of the data. Low levels of noise results in least square estimation, whereas higher levels of noise result in robust processing. While processing data, biasing effect, caused by noise, must be removed.

4.2 1D and 2D Inversion modeling in WinGLink

Once time series are looking better, the data are imported into a different software, which is WinGLink (Schlumberger Limited, 2015). The WinGLink software processes, interprets and produces models for AMT data and data from other geophysical disciplines (Schlumberger Limited, 2015). It produces maps and cross-sections of the data. WinGLink converts all the impedance files to a different file format (.edi). Apparent resistivity graph (Ωm), phase (deg), the strike (azimuth) (deg), and dimensional parameters are plotted against log10Period (see Figure 7). The software makes maps that show contoured and color-coded maps (Schlumberger Limited, 2015). It models resistivity at constant elevation or depth in 1D or 2D for AMT and MT data. Parameters include apparent resistivity, phase, tipper magnitude and strike, impedance rotation, and skew, where period is constant. WinGLink produces Occam and Bostick 1D models and exports EDI files (Schlumberger Limited, 2015). For this project, the goal is to make 1D and 2D inversions, using the WinGLink software. This will give a model of the variations in the resistivity structure with depth (1D) and along profile (2D). 1D modeling allows for changing in the resistivity with depth only (Flóvenz et al., 2012), assuming horizontal layers, while 2D modeling allows for changing in the resistivity with two directions: with depth and along the profile.

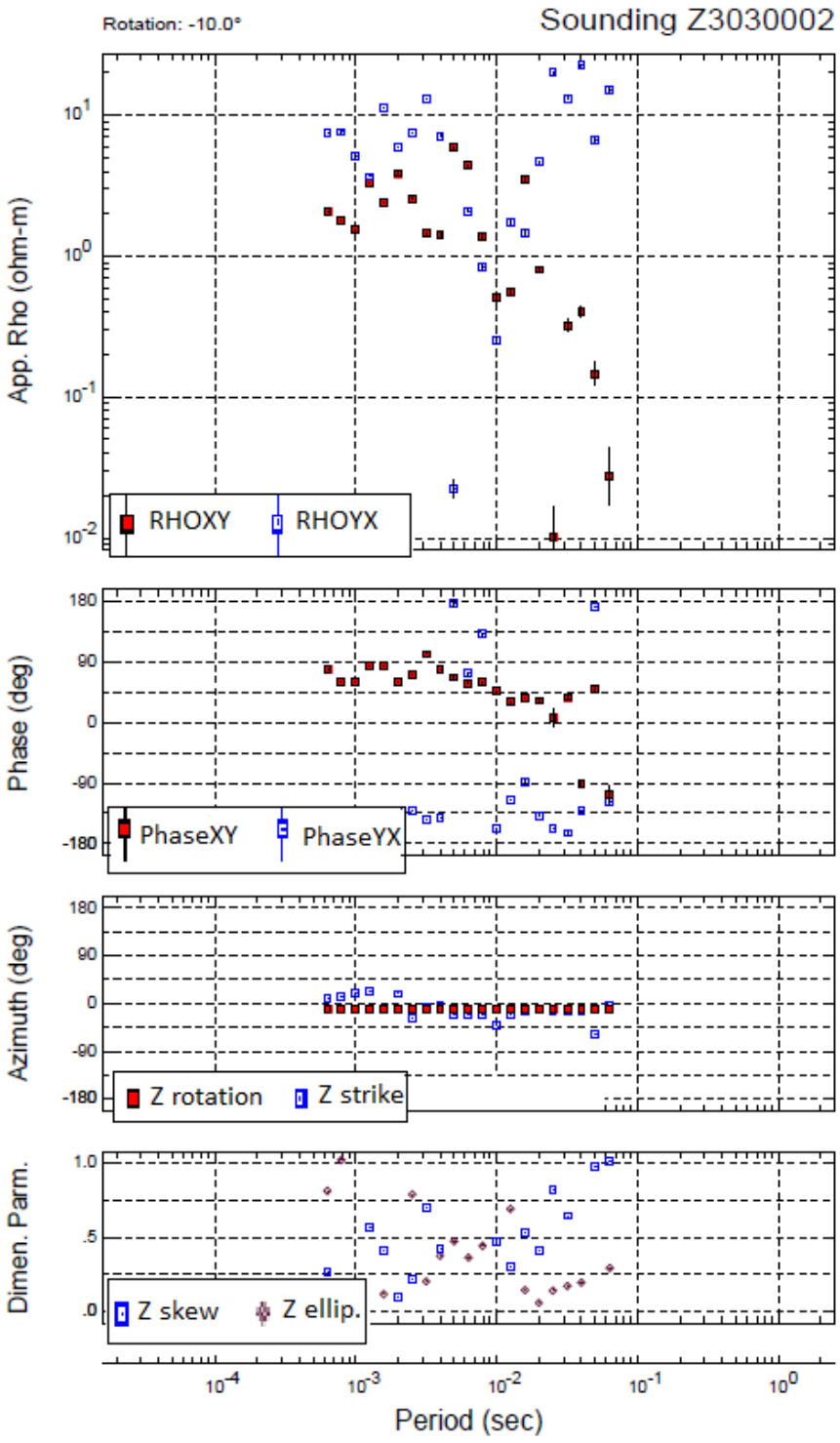

Figure 7: Interpretational quantities plotted against Period (s) in WinGLink. Apparent resistivits in both East-West (XY) and North-South (YX) directions are represented with red and blue squares in the top graph; Phases in both East-West (XY) and North-South (YX) directions are represented with red and blue squares in the second graph; Azimuths (Z rotation and Z strike) are represented with red and blue squares in the third graph; and Dimensional Parameters (Z skewness and Z ellipses) are represented with red and blue squares in the bottom graph.

It is important that the effect of aliasing is taken into account when interpreting the data. That is when the frequency appears to be lower than it truly is; aliasing is caused by under-sampling in the time or space domain (Simpson & Bahr, 2005). An anti-alias filter must be applied to the data to remove energy above Nyquist frequency, which relates to the sampling period as follows:

$$\omega_{NY} = 2\pi/2\Delta t \tag{15}$$

Where ω_{NY} is the Nyquist frequency and Δt is the sampling period. The Nyquist frequency has twice the value of the sampling frequency; if the intervals of a time series is Δt, then the Nyquist period is $2\Delta t$. This period is the period of when the signals in the time series are surely solved. Another important concept is the so called dead-band, when working through the data sets. At frequencies about 1-5 kHz signal amplitudes are attenuated, this frequency range is referred to as the AMT dead-band (Chave & Jones, 2012); this is when natural electromagnetic fluctuations are of lower amplitude than other ranges in the power spectrum. As a result of the dead band, the quality of AMT data reduces.

4.3 Preliminary Results from Waianae

Results were obtained from Waiʻanae Range, Oʻahu, Hawaiʻi Island. The results are displayed on a map, where all AMT profiles are presented. For all AMT sites measured, raw plots are produced, where interpretational quantities, such as apparent resistivity and phase are plotted against a range of frequency on a logarithmic scale.

Table 2: Project's sites in a table

Site ID	Date of survey	Longitude (UTM)	Latitude (UTM)	Elevation (m)	Transmitter
Lualualei Valley					
LLL006	6/4/2015	590410	2372526	97	N/A
LLL010	6/5/2015	590204	2370779	80	N/A
LLL009	6/5/2015	590225	2371371	80	N/A
LLL008	6/5/2015	590317	2371919	83	N/A
LLL007	6/5/2015	590531	2372957	106	N/A
LLL001	6/6/2015	590553	2373491	122	N/A
LLL002	6/6/2015	591147	2373611	308	N/A
LLL017	6/9/2015	589045	2367099	60	N/A
LLL018	6/9/2015	589090	2366611	70	N/A
LLL019	6/10/2015	589111	2365951	55	Yes
LLL020	6/10/2015	588796	2365577	43	Yes
Schofield Barracks					
SCH001	5/2/2016	591820	2374994	462	N/A
SCH002	5/2/2016	591913	2375311	494	N/A
SCH003	5/4/2016	592056	2375740	438	N/A
SCH004	5/4/2016	592267	2376101	427	N/A
Waianae Kai					
WK001	6/11/2015	588152	2374662	180	N/A
WK002	6/11/2015	587659	2375057	211	N/A
WK003	6/11/2015	587537	2373621	127	N/A
WK004	5/10/2016	587286	2375571	277	N/A
WK005	5/12/2016	587064	2375924	333	N/A
WK006	5/13/2016	587234	2376821	471	N/A
WK007	5/13/2016	587325	2377136	511	N/A

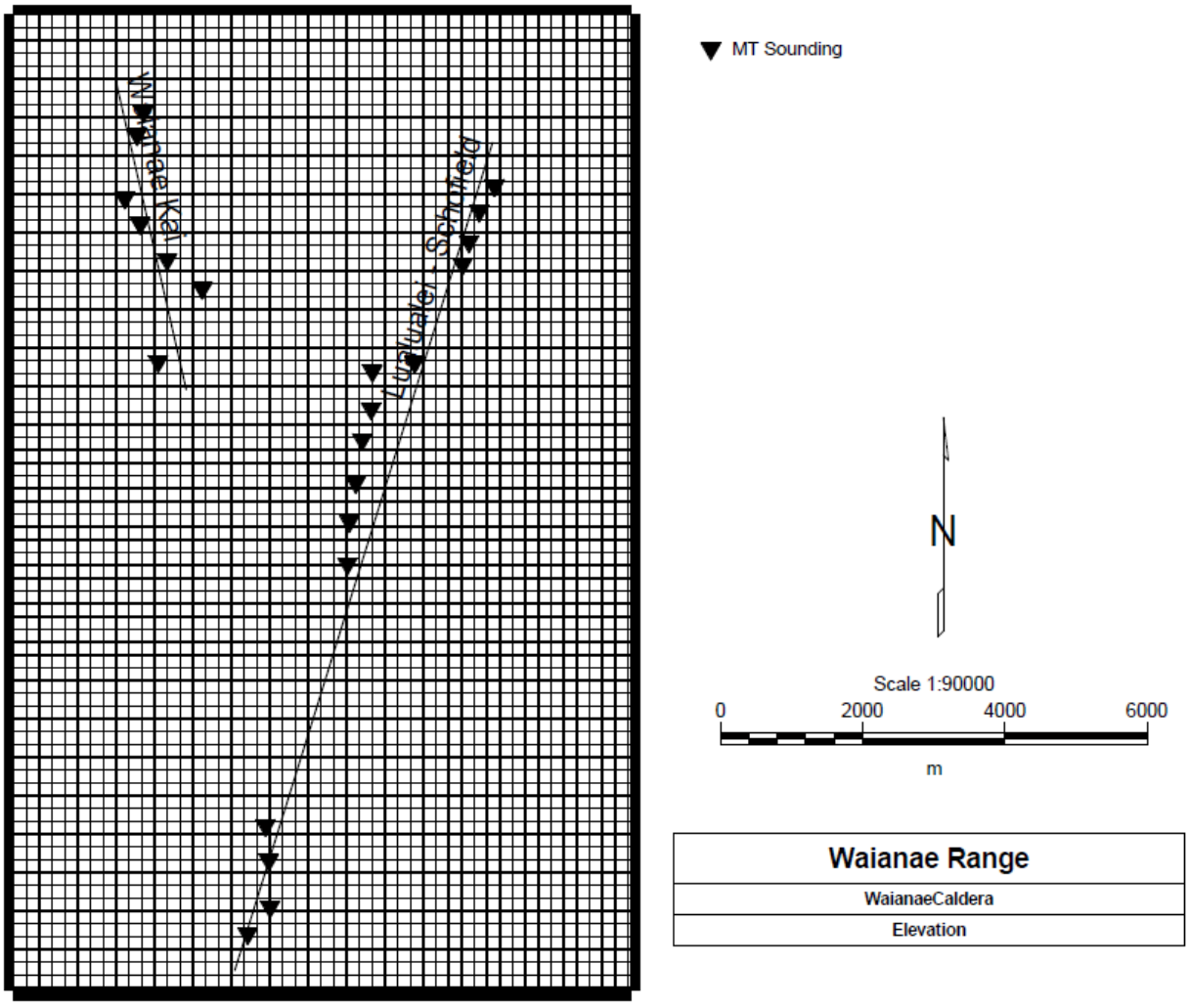

Figure 8: Map showing two profiles of the sites measured across Waianae Range (Lualualei Valley to Schofield Barracks, Oahu, Hawaii) and up in Waianae Kai.

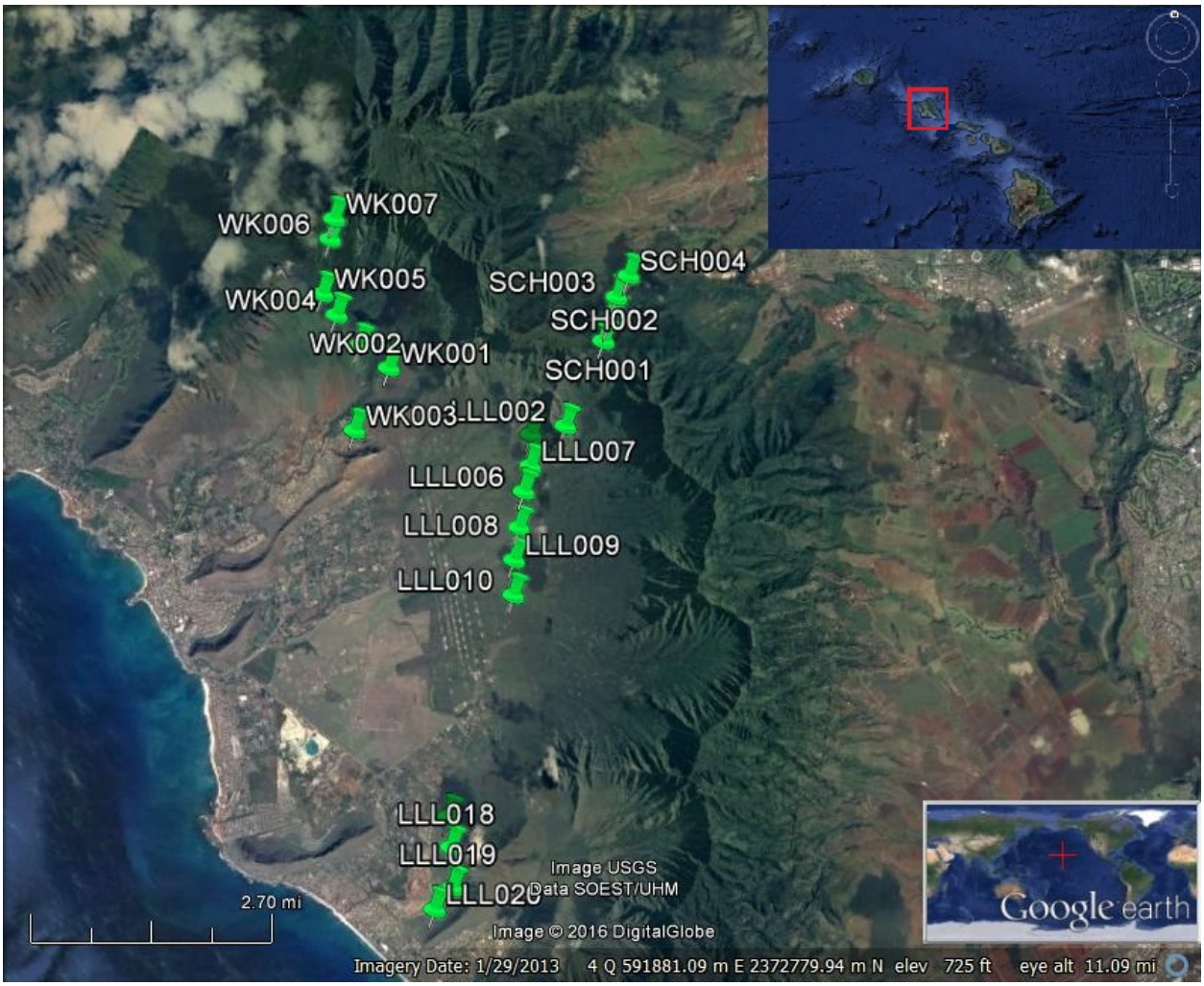

Figure 9: Locations of the AMT measurements displayed with green pins on a map in Google Earth. Location coordinates are listed in the previous table.

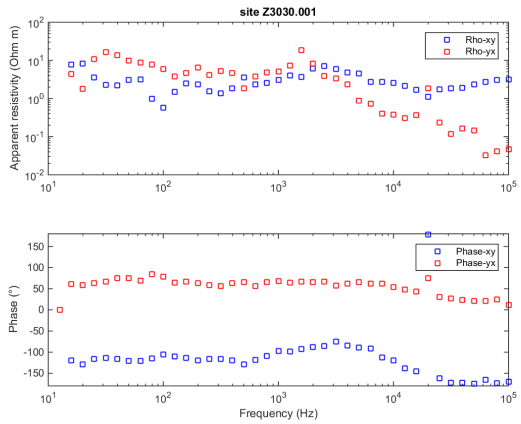

(a) Apparent resistivity and phase for site `Z3030.001` vs. frequency.

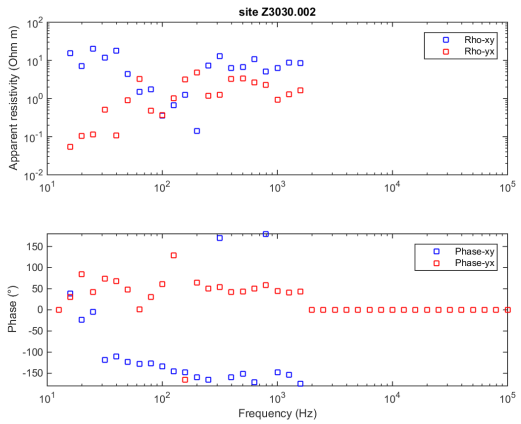

(b) Apparent resistivity and phase for site `Z3030.002` vs. frequency.

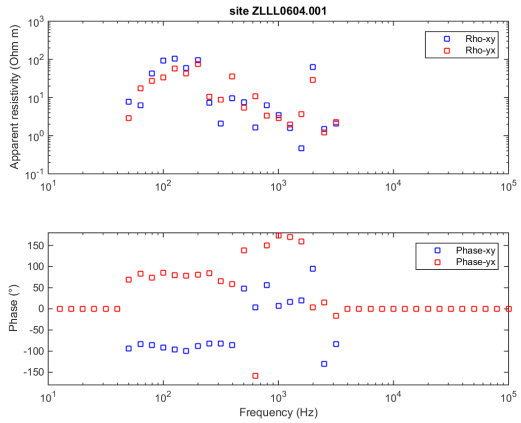

(c) Apparent resistivity and phase for site `ZLLL0604.001` vs. frequency.

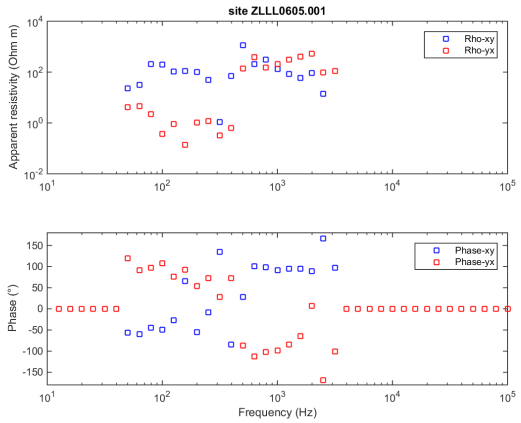

(d) Apparent resistivity and phase for site `ZLLL0605.001` vs. frequency.

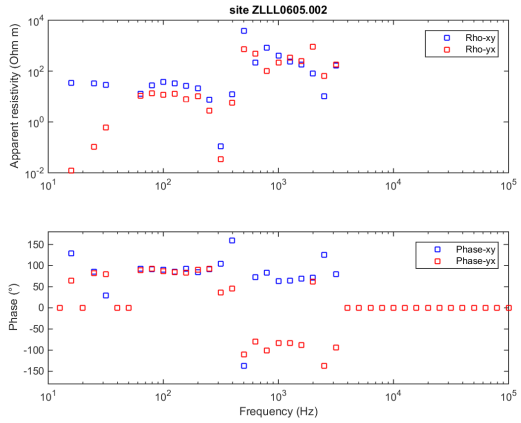

(e) Apparent resistivity and phase for site `ZLLL0605.002` vs. frequency.

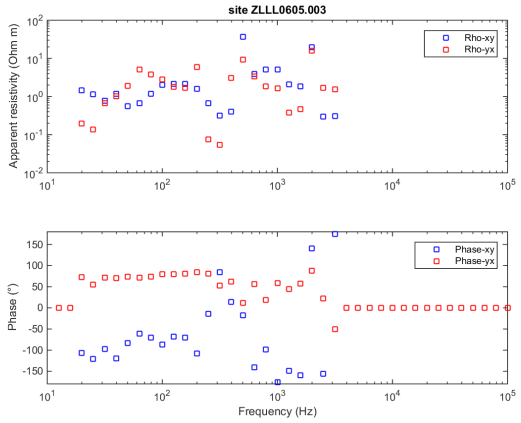

(f) Apparent resistivity and phase for site `ZLLL0605.003` vs. frequency.

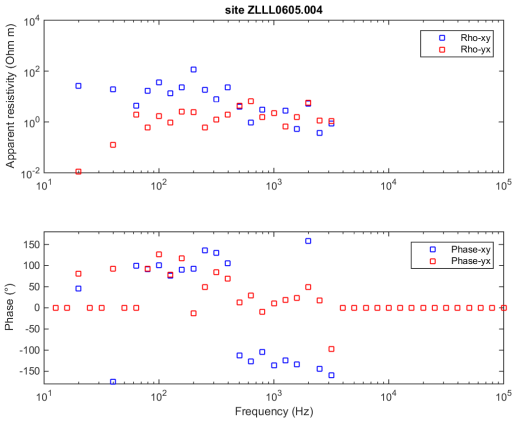

(g) Apparent resistivity and phase for site `ZLLL0605.004` vs. frequency.

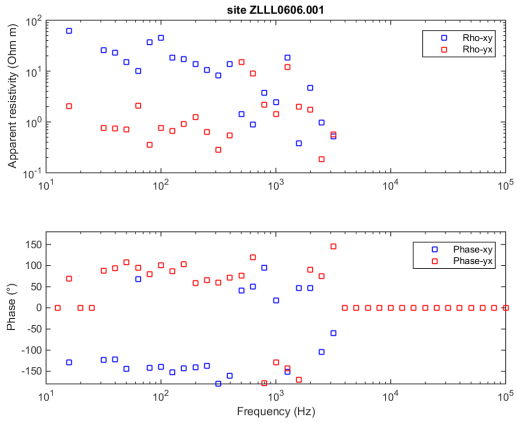

(h) Apparent resistivity and phase for site `ZLLL0606.001` vs. frequency.

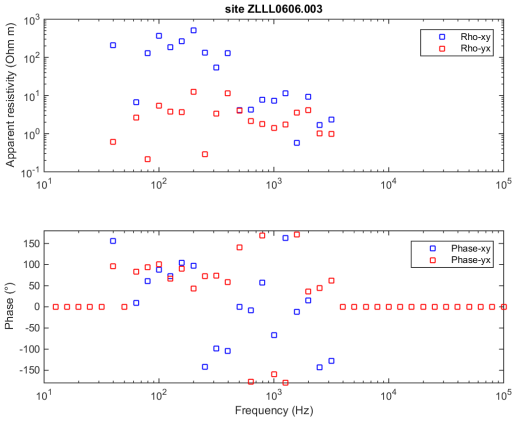

(i) Apparent resistivity and phase for site `ZLLL0606.003` vs. frequency.

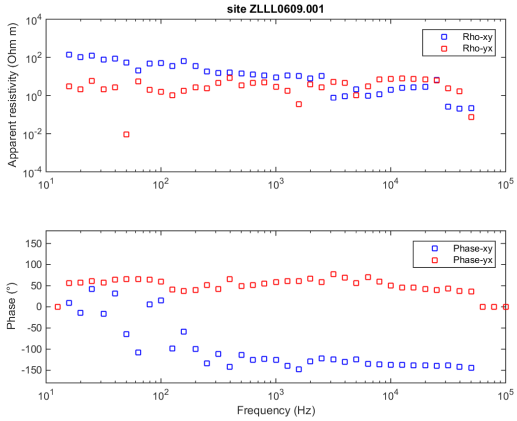

(j) Apparent resistivity and phase for site `ZLLL0609.001` vs. frequency.

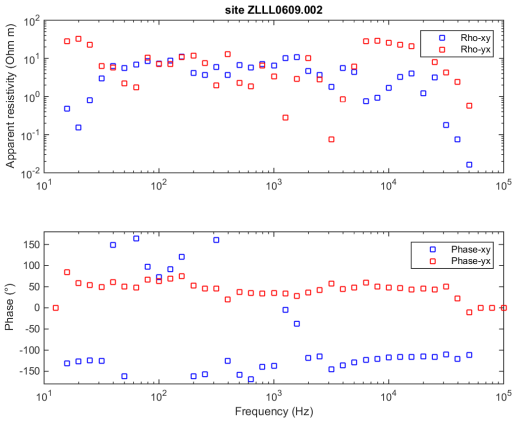

(k) Apparent resistivity and phase for site `ZLLL0609.002` vs. frequency.

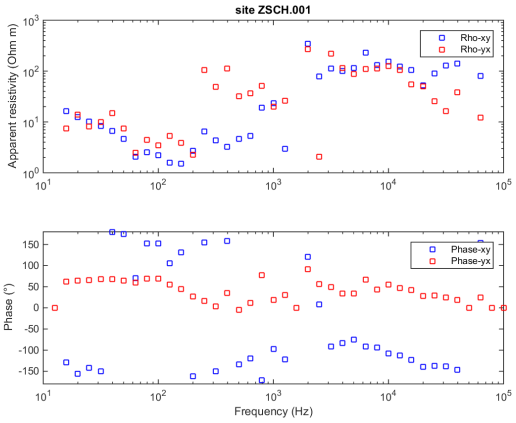

(l) Apparent resistivity and phase for site `ZSCH.001` vs. frequency.

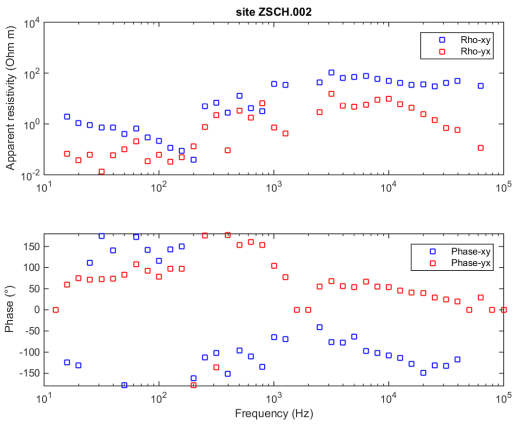

(m) Apparent resistivity and phase for site `ZSCH.002` vs. frequency.

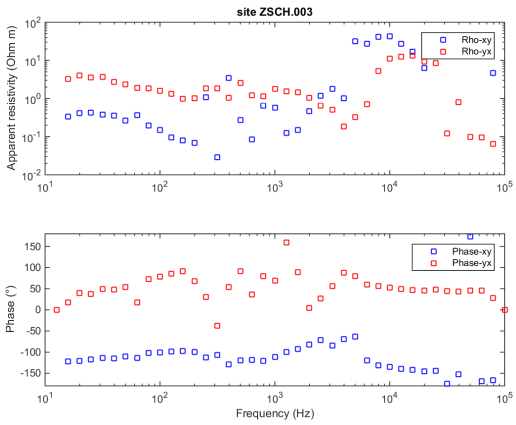

(n) Apparent resistivity and phase for site `ZSCH.003` vs. frequency.

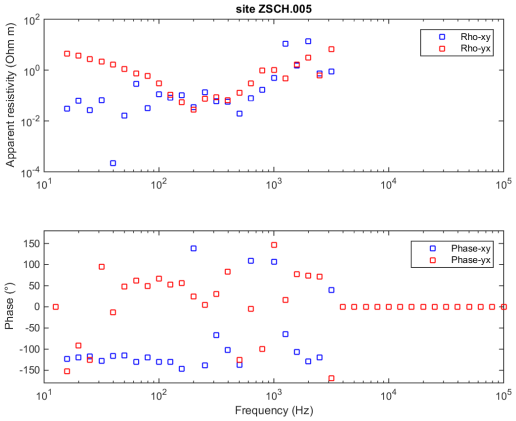

(o) Apparent resistivity and phase for site `ZSCH.005` vs. frequency.

Figure 10: Plots for AMT data in the frequency domain, from Lualualei-Schofield profile. Apparent resistivity and phase are displayed as a function of frequency. Blue squares represent resistivity and phase for TE mode (xy) and the red squares represent the resistivity and phase curves for the TM mode (yx).

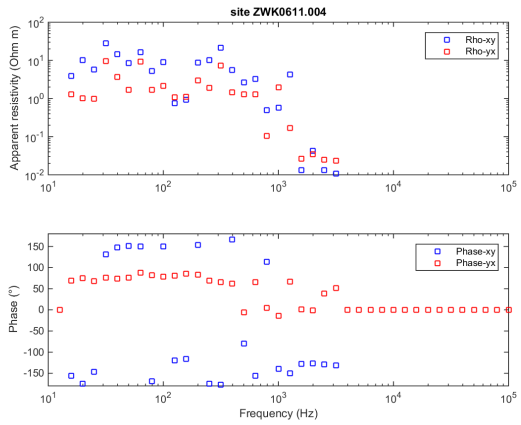

(a) Apparent resistivity and phase for site `ZWK0611.004` vs. frequency.

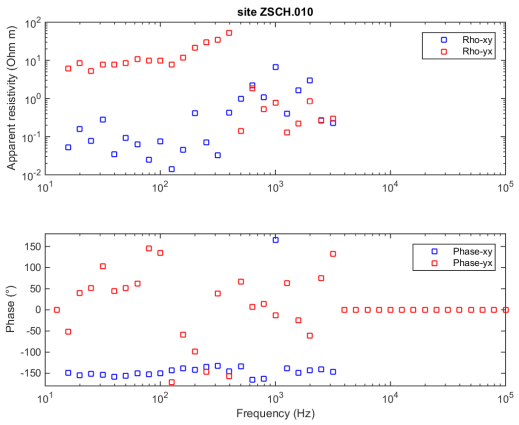

(b) Apparent resistivity and phase for site `ZSCH.010` vs. frequency.

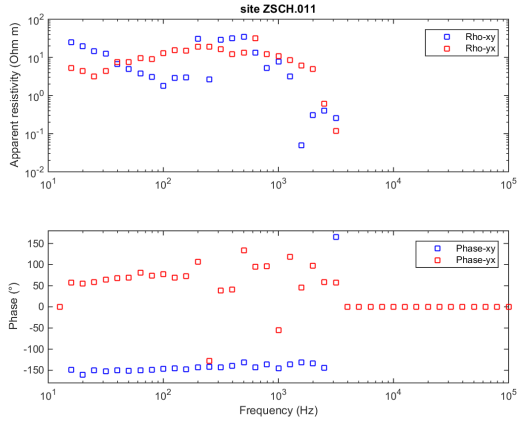

(c) Apparent resistivity and phase for site `ZSCH.011` vs. frequency.

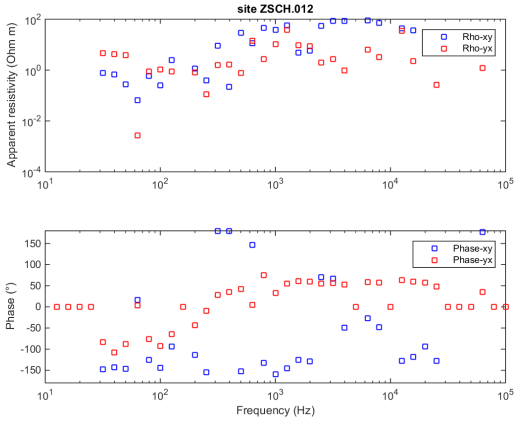

(d) Apparent resistivity and phase for site `ZSCH.012` vs. frequency.

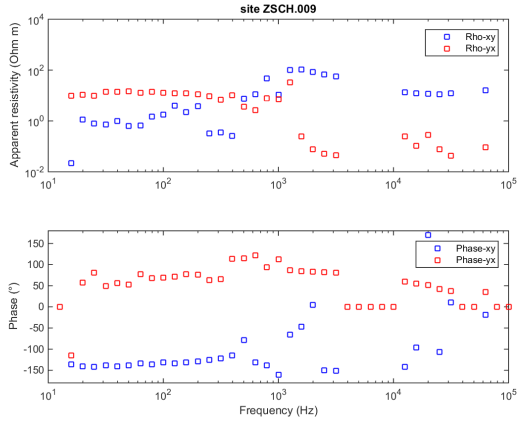

(e) Apparent resistivity and phase for site `ZSCH.009` vs. frequency.

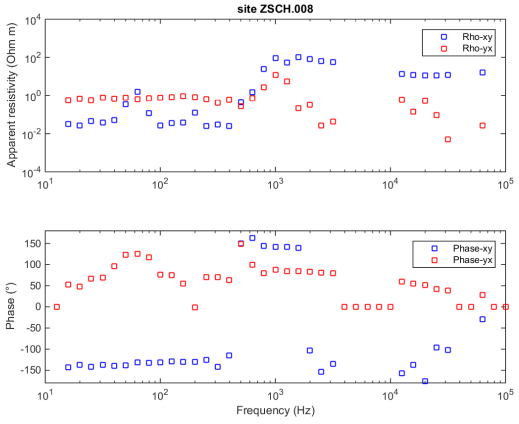

(f) Apparent resistivity and phase for site `ZSCH.008` vs. frequency.

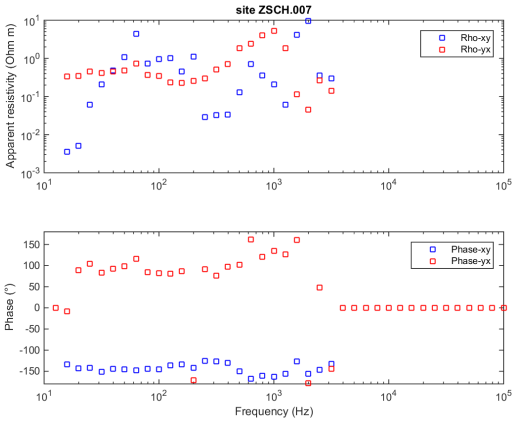

(g) Apparent resistivity and phase for site `ZSCH.007` vs. frequency.

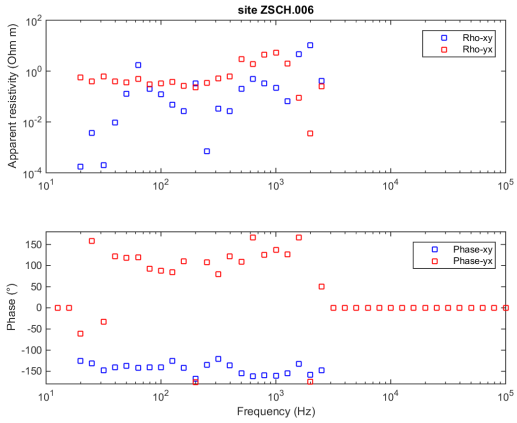

(h) Apparent resistivity and phase for site `ZSCH.006` vs. frequency.

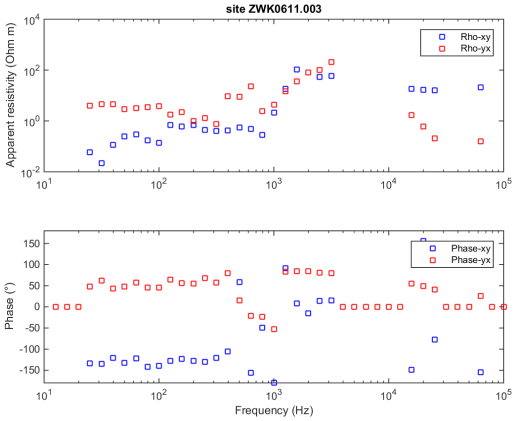

(i) Apparent resistivity and phase for site `ZWK0611.003` vs. frequency.

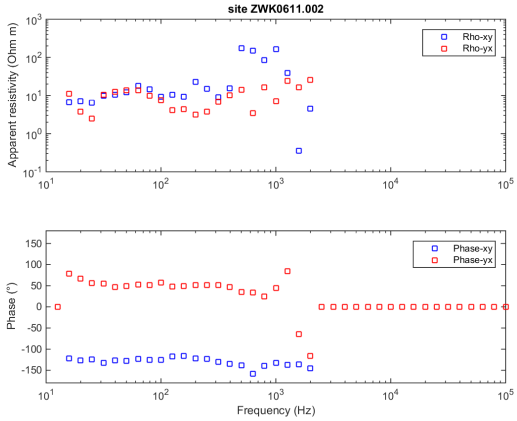

(j) Apparent resistivity and phase for site `ZWK0611.002` vs. frequency.

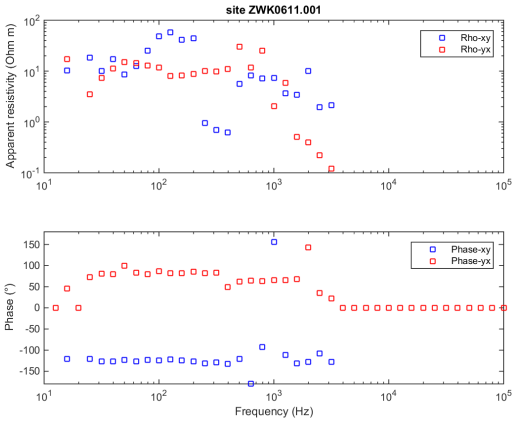

(k) Apparent resistivity and phase for site `ZWK0611.001` vs. frequency.

Figure 11: Plots for AMT data in the frequency domain, from Wainae Kai profile. Apparent resistivity and phase are displayed as a function of frequency. Blue squares represent resistivity and phase for TE mode (xy) and the red squares represent the resistivity and phase curves for the TM mode (yx).

References

Adams, W., & Furumoto, A. (1965). A seismic refraction study of the koolau volcanic plug. *Pacific Science*, *19*(3), 296.

Adams, W. M., Peterson, F. L., Mathur, S. P., Lepley, L., Warren, C., & Huber, R. D. (1969, September). *WRRCTR No. 32 A Hydrogeophyscial Survey from Kawaihae to Kailua-Kona, Hawaii* (Report). Water Resources Research Center, University of Hawaii at Manoa. Retrieved 2016-06-01, from `http://scholarspace.manoa.hawaii.edu/handle/10125/18093`

Anderson, L. (1984, January). Self-potential investigations in the Puhimau thermal area, Kilauea Volcano, Hawaii. *SEG Technical Program Expanded Abstracts 1984*, 1984.

Bartel, L., & Jacobson, R. (1987). Results of a controlled-source audiofrequency magnetotelluric survey at the puhimau thermal area, kilauea volcano, hawaii. *Geophysics*, *52*(5), 665-677.

Cagniard, L. (1953). Basic theory of the magneto-telluric method of geophysical prospecting. *Geophysics*, *18*, 605-635.

Chave, A., & Jones, A. (Eds.). (2012). *The magnetotelluric method: Theory and practice*. Cambridge University Press, New York.

Clague, D., & Sherrod, D. (2014). Characteristics of Hawaiian Volcanoes. In M. Poland, T. Takahashi, & C. Landowski (Eds.), (p. 97-146). U.S. Department of Interior, U.S. Geological Survey.

Constable, C. (2016). Surveys in geophysics. In (Vol. 37, p. 27-45). •.

Doell, R., & Dalrymple, G. (1973). Potassium-argon ages and paleomagnetism of the waianae and koolau volcanic series, oahu, hawaii. *Geological Society of America Bulletin*, *84*, 1217-1242.

Egbert, G. D., & Kelbert, A. (2012, April). Computational recipes for electromagnetic inverse problems. *Geophysical Journal International*, *189*(1), 251–267. Retrieved 2016-06-07, from `http://gji.oxfordjournals.org/content/189/1/251` doi: 10.1111/j.1365-246X.2011.05347.x

Flóvenz, G., Hersir, G., Sæmundsson, K., Ármannsson, H., & Friðriksson, T. (2012). Geothermal energy exploration techniques. sayigh, a., (ed.) comprehensive renewable energy. *Elevier, Oxford*, *7*, 51-95.

Funkhouser, J. G., Barnes, I. L., & Naughton, J. J. (1968). The Determination of a Series of Ages of Hawaiian Volcanoes by the Potassium-Argon Method! *Pacific Science*, *22*, 369-372. Retrieved from `http://scholarspace.manoa.hawaii.edu/handle/10125/7127`

Gamble, T. D., Goubau, W. M., & Clarke, J. (1979). Magnetotellurics with a remote magnetic reference. *Geophysics*, *44*(1), 53-68.

GEOMETRICS, I. (2007). Operation manual for stratagem system running imagem (2.19 ed.) [Computer software manual]. 2190 Fortune Drive, San Jose, CA 95131, USA.

Grose, L., & Keller, G. (1975). Geothermal energy in the pacific region appendix a: Exploration for a geothermal system in lualualei valley, oahu, hawaii. *ONR Report for Contract number N00014-71-A-0430-0004*.

Guillou, H., Sinton, J., Laj, C., Kissel, C., & Szeremeta, N. (2000, March). New K–Ar ages of shield lavas from Waianae Volcano, Oahu, Hawaiian Archipelago. *Journal of Volcanology and Geothermal Research*, *96*(3–4), 229–242. Retrieved 2016-07-26, from http://www.sciencedirect.com/science/article/pii/S0377027399001535 doi: 10.1016/S0377-0273(99)00153-5

Jackson, D., Kauahikaua, J., & Zablocki, C. (1985, December). Resistivity monitoring of an active volcano using the controlled-source electromagnetic technique: Kilauea, Hawaii. *Journal of Geophysical Research: Solid Earth*, *90*(B14), 12545–12555. Retrieved 2016-06-02, from http://onlinelibrary.wiley.com.eres.library.manoa.hawaii.edu/doi/10.1029/JB090iB14p12545/abstract doi: 10.1029/JB090iB14p12545

Jackson, D., & Sako, M. (1983). *Self-potential surveys related to probable geothermal anomalies, hualalai volcano, hawaii.* (U.S. Geological Survey, Open-file report 82-127, Hawaii National Park, HI)

Kauahikaua, J. (1981). *Interpretation of time-domain electromagnetic soundings in the east rift geothermal area of kilauaea volcano, hawaii* (Tech. Rep.). U.S. Department of the Interior, Geological Survey. (Open-file report 81-979)

Kelbert, A., & Egbert, G. (2011). *ModEM: User's Guide.*

Kelbert, A., Meqbel, N., Egbert, G. D., & Tandon, K. (2014, May). ModEM: A modular system for inversion of electromagnetic geophysical data. *Computers & Geosciences*, *66*, 40–53. Retrieved 2016-06-10, from http://www.sciencedirect.com/science/article/pii/S0098300414000211 doi: 10.1016/j.cageo.2014.01.010

Key, K., Constable, S., Liu, L., & Pommier, A. (2013, March). Electrical image of passive mantle upwelling beneath the northern east pasific rise. *Nature*, *495*(7442), 499.

Laj, C., Guillou, H., Szeremeta, N., & Coe, R. (1999, July). Geomagnetic paleosecular variation at Hawaii around 3 Ma from a sequence of 107 lava flows at Kaena Point (Oahu). *Earth and Planetary Science Letters*, *170*(4), 365–376. Retrieved 2016-10-12, from http://www.sciencedirect.com/science/article/pii/S0012821X99001193 doi: 10.1016/S0012-821X(99)00119-3

Malahoff, A., & Woollard, G. (1966). Magnetic measurements over the hawaiian ridge and their volcanological implications. *Bulletin Volcanology*.

Mattice, M. (1981). *Geothermal and ground water exploration on maui, hawaii, by applying d.c. electrical soundings* (Unpublished master's thesis). University of Hawaii, Honolulu.

McDougall, I. (1964). Potassium-Argon Ages from Lavas of the Hawaiian Islands. *Geological Society of America Bulletin*, *75*(2), 107–128. Retrieved from http://gsabulletin.gsapubs.org.eres.library.manoa.hawaii.edu/content/75/2/107 doi: 10.1130/0016-7606(1964)75[107:PAFLOT]2.0.CO;2

Moore, J. G., Clague, D. A., Holcomb, R. T., Lipman, P. W., Normark, W. R., & Torresan, M. E. (1989, December). Prodigious submarine landslides on the Hawaiian Ridge. *Journal of Geophysical Research: Solid Earth*, *94*(B12), 17465–17484. Retrieved 2016-10-12, from http://onlinelibrary.wiley.com.eres.library.manoa.hawaii.edu/doi/10.1029/JB094iB12p17465/abstract doi: 10.1029/JB094iB12p17465

Naidu, G. (2012). Deep crustal structure of the son-narmada-tapti linement. In (p. 13-39). Springer-Verlag Berlin Heidelberg.

Pierce, H., & Thomas, D. (2009). *Magnetotelluric and audiomagnetotellurics groundwater survey along the Humu'ula portion of Saddle Road near and around the Pohakuloa Training Area, Hawaii (ver 1.1).* (160 p. Open-file report 2009-1135)

Presley, T., Sinton, J., & Pringle, M. (1997). Postshield volcanism and catastrophic mass wasting of the waianae volcano, oahu, hawaii. *Bulletin of Volcanology*, *58*, 597-616.

Schlumberger Limited. (2015). *WinGLink Software.* Retrieved from http://www.slb.com/services/seismic/geophysical_processing_characterization/seismic_reservoir_characterization/electromagnetics/emsoftware/winglink.aspx

Sherrod, D., Sinton, J., Watkins, S., & Brunt, K. (2007). *Geologic map of the state of Hawai'i.* (Open-file Report 2007-1089, available only at http://pubs.usgs.gov/of.2007/1089/)

Simpson, F., & Bahr, K. (2005). *Practical magnetotellurics.* Press Syndicate of the University of Cambridge, United Kingdom.

Sinton, J. (1986). Revision of stratigraphic nomenclature of waianae volcano, oahu, hawaii. *U.S. Geological Survey Bulletin 1775-A*, A9-A15.

Sinton, J., Eason, D., Tardona, M., Pyle, D., van der Zander, I., Guillou, H., ... Mahoney, J. (2014). Ka‘ena Volcano—A precursor volcano of the island of O‘ahu, Hawai‘i. *Geological Society of America Bulletin*, *126*(9-10), 1219–1244. doi: 10.1130/B30936.1

Siripunvaraporn, W. (2012). Three-Dimensional Magnetotelluric Inversion: An Introductory Guide for Developers and Users. *Surv Geophys*, *33*, 5-27.

Stearns, H., & Vaksvik, K. (1935). Geology and ground-water resources of the Island of Oahu, Hawaii. *U.S. Geological Survey*, *1*, 1-479.

Strange, W., Machesky, L., & Woollard, G. (1965). A gravity survey of the island of oahu, hawaii. *Pacific Science*, *19*(3), 350-353.

Thomas, D., Cox, M., & Kajiwara, L. (1979). Potential geothermal resources in Hawaii: A preliminary regional survey. *Assessment of Geothermal Resources in Hawaii*(1). (Phase 1, Final Report)

Tikhonov, A. (1950). On determining electrical characteristics of the deep layers of the Earth's crust. *Doklady*, *73*(2), 295-297.

van der Zander, I., Sinton, J., & Mahoney, J. (2010). Late Shield-Stage Silicic Magmatism at Wai'anae Volcano: Evidence for Hydrous Crustal Melting in Hawaiian Volcanoes. *Journal of Petrology*, *51*(3), 671-701.

Vozoff, K. (1972). The magnetotelluric method in the exploration of sedimentary basins. *GEOPHYSICS*, *37*(1), 98-141.

Vozoff, K. (1990). Magnetotellurics: Principles and practice. *Proc. Indian Acad. Sci. (Earth Planet. Sci.)*, *99*(4), 441-471.

Wolfe, E., Wise, W., & Dalrymple, G. (1997). The geology and petrology of Mauna Kea Volcano, Hawaii – A study of Postshield Volcanism. *U.S. Geological Survey professional paper 1557, Denver*.

Zablocki, C. (1976a). Mapping thermal anomalies on an active volcano by self-potential method, Kilauea, Hawaii. In *In proc. 2nd U.N. Symp. on the Development and Use of Geothermal Resources.*

Zablocki, C. (1976b). *Some electrical and magnetic studies of Kilauea Iki lava lake, Hawaii* (Tech. Rep.). U.S. Geological Survey. (Open-file report 76-304)

Zbinden, E., & Sinton, J. (1988). Dikes and the petrology of waianae volcano, oahu. *Journal of Geophysical Research: Solid Earth*, *93*(B12), 14856-14866.

Zohdy, A., & Jackson, D. (1969). Application of deep electrical soundings for groundwater exploration in hawaii. *Geophysics*, *34*(4), 584-600.

Appendices

A Maxwell's derivations

In this appendix, the solutions for the electric and magnetic fields will be derived from the Faraday's and Ampére's laws, which are given by the following

Faraday's law

$$\nabla \times \mathbf{E} = -\mu \frac{\partial \mathbf{H}}{\partial t} \tag{16}$$

Ampére's law

$$\nabla \times \mathbf{H} = \sigma \mathbf{E} + \epsilon \frac{\partial \mathbf{E}}{\partial t} \tag{17}$$

Equations 16 and 17 describe the relationship between the two fields, $\mathbf{E}$ and $\mathbf{H}$, where $\mathbf{E} = (E_x\hat{i}, E_y\hat{j}, E_z\hat{k})$ and $\mathbf{H} = (H_x\hat{i}, H_y\hat{j}, H_z\hat{k})$. Before solving for them, we assume for a plane wave

$$\frac{\partial}{\partial x} = \frac{\partial}{\partial y} = 0 \tag{18}$$

This demonstrates that there are no variations in the fields, except in depth, z. This problem will be solved in the frequency domain, which means we have to Fourier transform time dependent quantities to frequency dependent quantities. The Fourier transforms for a variable $x(t)$ and its time derivatives are given in the following equations

$$\mathcal{F}\{x(t)\} = \hat{x}(\omega) = \int_{-\infty}^{\infty} x(t) e^{-i\omega t} dt \tag{19}$$

$$\mathcal{F}\left\{x^{(n)}(t)\right\} = (i\omega)^n \hat{x}(\omega) = (i\omega)^n \int_{-\infty}^{\infty} x(t) e^{-i\omega t} dt \tag{20}$$

Where $\mathcal{F}$ is the Fourier transform operator, ω is the angular frequency, $x(t)$ is the variable in the time domain, and $\hat{x}(\omega)$ is the variable in the frequency domain. We start with the Faraday's law (eq. 16) and we use equations 19 and 20 to transform the variables into the Fourier domain.

$$\mathcal{F}\{\nabla \times \mathbf{E}\} = \mathcal{F}\left\{\left(\frac{\partial E_z}{\partial y} - \frac{\partial E_y}{\partial z}\right)\hat{i} + \left(\frac{\partial E_x}{\partial z} - \frac{\partial E_z}{\partial x}\right)\hat{j} + \left(\frac{\partial E_y}{\partial x} - \frac{\partial E_x}{\partial y}\right)\hat{k}\right\} = \mathcal{F}\left\{-\mu \frac{\partial \mathbf{H}}{\partial t}\right\} \tag{21}$$

which then becomes

$$\mathcal{F}\left\{\left(-\frac{\partial E_y}{\partial z}\right)\hat{i}+\left(\frac{\partial E_x}{\partial z}\right)\hat{j}\right\}=-\mu\mathcal{F}\left\{\frac{\partial \mathbf{H}}{\partial t}\right\} \tag{22}$$

Because of the plane wave assumption, terms dependent on either x or y are zero. For solutions in $\hat{\mathbf{i}}$ and $\hat{\mathbf{j}}$ direction we arrive at

$$\mathcal{F}\left\{\frac{\partial E_y}{\partial z}\right\}=\frac{\partial}{\partial z}\hat{E}_y(\omega)=\mu i\omega\hat{H}_x(\omega) \tag{23}$$

$$\mathcal{F}\left\{\frac{\partial E_x}{\partial z}\right\}=\frac{\partial}{\partial z}\hat{E}_x(\omega)=-\mu i\omega\hat{H}_y(\omega) \tag{24}$$

The derivatives of equations 23 and 24 with respect to z are

$$\frac{\partial}{\partial z}\left(\frac{\partial \hat{E}_y(\omega)}{\partial z}\right)=\frac{\partial}{\partial z}\left(\mu i\omega\hat{H}_x(\omega)\right)$$

$$\frac{\partial^2 \hat{E}_y(\omega)}{\partial z^2}=\mu i\omega\frac{\partial \hat{H}_x(\omega)}{\partial z} \tag{25}$$

and

$$\frac{\partial}{\partial z}\left(\frac{\partial \hat{E}_x(\omega)}{\partial z}\right)=\frac{\partial}{\partial z}\left(\mu i\omega\hat{H}_y(\omega)\right)$$

$$\frac{\partial^2 \hat{E}_x(\omega)}{\partial z^2}=\mu i\omega\frac{\partial \hat{H}_y(\omega)}{\partial z} \tag{26}$$

Now, to find $\frac{\partial \hat{H}_x(\omega)}{\partial z}$ and $\frac{\partial \hat{H}_y(\omega)}{\partial z}$, we start deriving from Ampére's law (equation 17)

$$\nabla\times\mathbf{H}=\left(\frac{\partial H_z}{\partial y}-\frac{\partial H_y}{\partial z}\right)\hat{i}+\left(\frac{\partial H_x}{\partial z}-\frac{\partial H_z}{\partial x}\right)\hat{j}+\left(\frac{\partial H_y}{\partial x}-\frac{\partial H_x}{\partial y}\right)\hat{k}=\sigma\mathbf{E}+\epsilon\frac{\partial \mathbf{E}}{\partial t}$$

and once again, we lose x and y terms here and get

$$\nabla\times\mathbf{H}=\left(-\frac{\partial H_y}{\partial z}\right)\hat{i}+\left(\frac{\partial H_x}{\partial z}\right)\hat{j}=\sigma\mathbf{E}+\epsilon\frac{\partial \mathbf{E}}{\partial t} \tag{27}$$

We Fourier transform 27 with equations 19 and 20 into the frequency domain and obtain the following

$$\mathcal{F}\left\{\left(-\frac{\partial H_y}{\partial z}\right)\hat{i}+\left(\frac{\partial H_x}{\partial z}\right)\hat{j}\right\}=\mathcal{F}\left\{\sigma\mathbf{E}+\epsilon\frac{\partial \mathbf{E}}{\partial t}\right\} \tag{28}$$

$$-\frac{\partial \hat{H}_y(\omega)}{\partial z}=\sigma\hat{E}_x(\omega)+\epsilon i\omega\hat{E}_x(\omega)$$

$$\frac{\partial \hat{H}_y(\omega)}{\partial z}=-(\sigma+i\omega\epsilon)\hat{E}_x(\omega) \tag{29}$$

$$\frac{\partial \hat{H}_x(\omega)}{\partial z}=\sigma\hat{E}_y(\omega)+\epsilon i\omega\hat{E}_y(\omega)$$

$$\frac{\partial \hat{H}_x(\omega)}{\partial z}=(\sigma+i\omega\epsilon)\hat{E}_y(\omega) \tag{30}$$

Now we substitute equations 29 and 30 into equations 25 and 26 and derive the ordinary differential equations (ODEs) for the electric (E) field

$$\frac{\partial^2 \hat{E}_y(\omega)}{\partial z^2}=\mu i\omega(\sigma+i\omega\epsilon)\hat{E}_y(\omega) \tag{31}$$

$$\frac{\partial^2 \hat{E}_x(\omega)}{\partial z^2}=\mu i\omega(\sigma+i\omega\epsilon)\hat{E}_x(\omega) \tag{32}$$

Where we define $k^2=\mu i\omega(\sigma+i\omega\epsilon)$, and equations 31 and 32 become

$$\frac{\partial^2 \hat{E}_y(\omega)}{\partial z^2}=k^2\hat{E}_y(\omega) \tag{33}$$

$$\frac{\partial^2 \hat{E}_x(\omega)}{\partial z^2}=k^2\hat{E}_x(\omega) \tag{34}$$

When solving the ODEs we guess that $\hat{E}_y(\omega)=e^{\lambda_y z}e^{i\omega t}$ and $\hat{E}_x(\omega)=e^{\lambda_x z}e^{i\omega t}$, as the fields are dependent on both frequency and depth. We get $\lambda_x=\lambda_y=\pm k$ and therefore arrive to the general solutions of

$$\hat{E}_y(\omega) = \left(A_x e^{kz} + B_x e^{-kz}\right) e^{i\omega t} \tag{35}$$

$$\hat{E}_x(\omega) = \left(C_y e^{kz} + D_y e^{-kz}\right) e^{i\omega t} \tag{36}$$

Now we want the limit of those solutions as z is large ($z \to \infty$) to equal zero

$$Lim_{z\to\infty} \left(A_x e^{kz} + B_x e^{-kz}\right) e^{i\omega t} = 0$$

$$Lim_{z\to\infty} \left(C_y e^{kz} + D_y e^{-kz}\right) e^{i\omega t} = 0 \tag{37}$$

For this to be true, $A_x = C_y = 0$ must also be true. Then we are left with

$$\hat{E}_y(\omega) = B_x e^{-kz} e^{i\omega t} \tag{38}$$

$$\hat{E}_x(\omega) = D_y e^{-kz} e^{i\omega t} \tag{39}$$

We join equations 38 and 39 to describe the whole field, which is given by $\hat{\mathbf{E}}(\omega) = (\hat{E}_y(\omega)\hat{i}, \hat{E}_x(\omega)\hat{j})$ and

$$\hat{\mathbf{E}}(\omega) = \hat{\mathbf{E}}_\mathbf{0} e^{-kz} e^{i\omega t}$$

where $\hat{\mathbf{E}}_\mathbf{0}$ is the initial amplitude at $t = z = 0$.

Now we get back to equations 29 and 30 and go through similar steps with them as with equations 23 and 24; we differentiate them with respect to z.

$$\frac{\partial}{\partial z}\left(\frac{\partial \hat{H}_y(\omega)}{\partial z}\right) = \frac{\partial}{\partial z}\left(-(\sigma + i\omega\epsilon)\hat{E}_x(\omega)\right)$$

$$\frac{\partial^2 \hat{H}_y(\omega)}{\partial z^2} = -(\sigma + i\omega\epsilon)\frac{\partial \hat{E}_x(\omega)}{\partial z} \tag{40}$$

We can substitute equation 23 into equation 40 and get

$$\frac{\partial^2 \hat{H}_y(\omega)}{\partial z^2} = \mu i\omega(\sigma + i\omega\epsilon)\hat{H}_y(\omega)$$

and with $k^2 = \mu i\omega(\sigma + i\omega\epsilon)$, we obtain

$$\frac{\partial^2 \hat{H}_y(\omega)}{\partial z^2} = k^2 \hat{H}_y(\omega) \tag{41}$$

Now for $\hat{H}_x$:

$$\frac{\partial}{\partial z}\left(\frac{\partial \hat{H}_x(\omega)}{\partial z}\right) = \frac{\partial}{\partial z}\left(-(\sigma + i\omega\epsilon)\hat{E}_y(\omega)\right)$$

$$\frac{\partial^2 \hat{H}_x(\omega)}{\partial z^2} = -(\sigma + i\omega\epsilon)\frac{\partial \hat{E}_y(\omega)}{\partial z} \tag{42}$$

We can substitute equation 24 into equation 44 and get

$$\frac{\partial^2 \hat{H}_x(\omega)}{\partial z^2} = k^2 \hat{H}_x(\omega) \tag{43}$$

Now that we have both ODEs for $\hat{\mathbf{H}}(\omega) = (\hat{H}_y(\omega)\hat{i}, \hat{H}_x(\omega)\hat{j})$ and

$$\frac{\partial^2 \hat{H}_y(\omega)}{\partial z^2} = k^2 \hat{H}_y(\omega) \tag{44}$$

$$\frac{\partial^2 \hat{H}_x(\omega)}{\partial z^2} = k^2 \hat{H}_x(\omega) \tag{45}$$

we follow the steps used from equations 33 and 34 to equations 38 and 39 and get the solution for equations 44 and 45 to be

$$\hat{\mathbf{H}}(\omega) = \hat{\mathbf{H}}_\mathbf{0} e^{-kz} e^{i\omega t}$$

where $\hat{\mathbf{H}}_\mathbf{0}$ is the initial amplitude, or when $z = t = 0$.

In this appendix we have derived the solutions for the fields from Faraday's and Ampére's laws (equations 16 and 17), assuming the electromagnetic wave to be a plane wave, and by Fourier transforming them from the time domain into frequency domain.

$$\hat{\mathbf{H}}(\omega) = \hat{\mathbf{H}}_\mathbf{0} e^{-kz} e^{i\omega t} \tag{46}$$

$$\hat{\mathbf{E}}(\omega) = \hat{\mathbf{E}}_\mathbf{0} e^{-kz} e^{i\omega t} \tag{47}$$

B Scanned Field work notes

The field notes have information about each site of this project, such as site names, file names, dates, UTM coordinates, notes of whether a transmitter was used during measurements, set gains, notes about the environment around the sites, a sketch describing the set up of the instrument specific to locations. Field crew: Telma Sigurdardottir and Cody Winchester.

B.1 Lualualei Valley

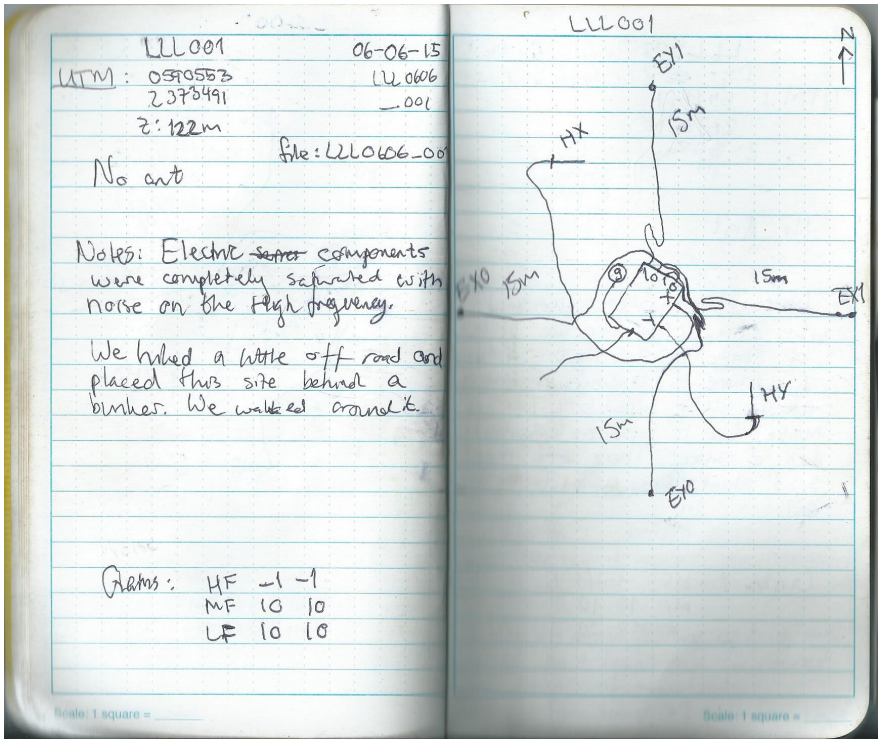

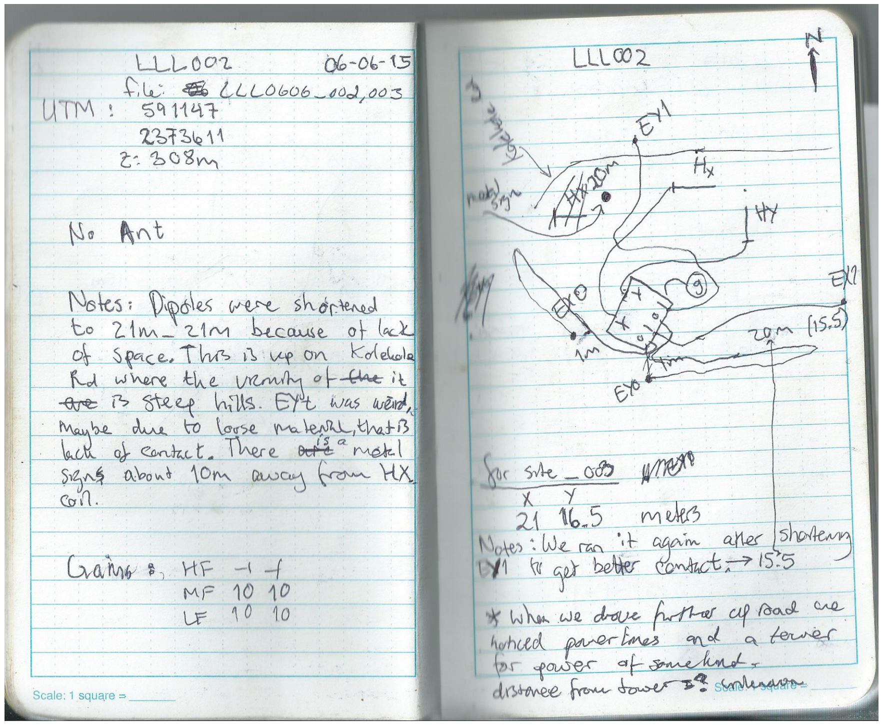
LLL002 06-06-15
file: ~~[illegible]~~ LLL0606_002,003
UTM: 591147
2373611
Z: 308m

No Ant

Notes: Dipoles were shortened to 21m_21m because of lack of space. This is up on Kolekole Rd where the vicinity of ~~the~~ it ~~are~~ is steep hills. EY1 was weird, maybe due to loose material, that is lack of contact. There ~~are~~ is a metal sign about 10m away from HX coil.

Gains: HF -1 -1
MF 10 10
LF 10 10

for site _003
X Y
21 16.5 meters
Notes: We ran it again after shortening EY1 to get better contact. → 15.5

* When we drove further up road we noticed powerlines and a tower for power of some kind. distance from tower ≈?

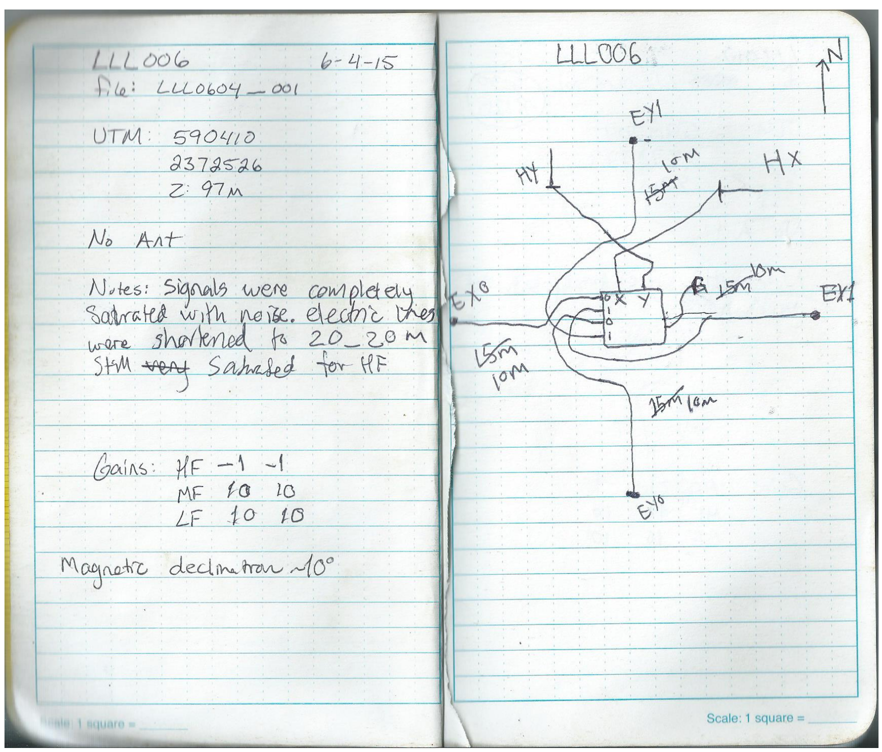
LLL006 6-4-15
file: LLL0604_001

UTM: 590410
2372526
Z: 97m

No Ant

Notes: Signals were completely Saturated with noise. electric lines were shortened to 20_20m Still ~~very~~ Saturated for HF

Gains: HF -1 -1
MF 10 10
LF 10 10

Magnetic declination ~10°

LLL007 06-05-15

file: LLL0605_004

UTM 590531
2372957
Z 106m

No Ant

Notes: —

Gains HF -1 -1
MF 10 10
LF 10 10

Scale: 1 square = _____

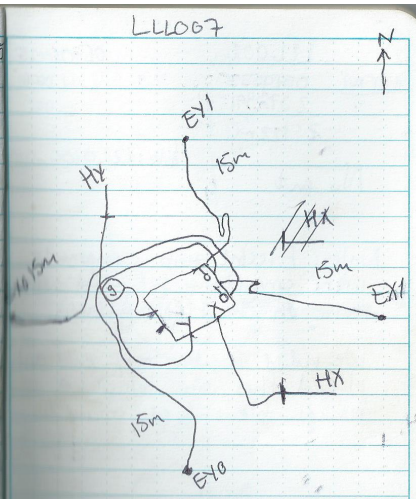

Scale: 1 square = _____

LLL008 06-05-15

file LLL0605_003

UTM 590317
2371919
Z: 83m

No Ant

Notes: less saturated than LLL009, but still bad.

Gains: HF -1 -1
MF 10 10
LF 10 10

Scale: 1 square = _____

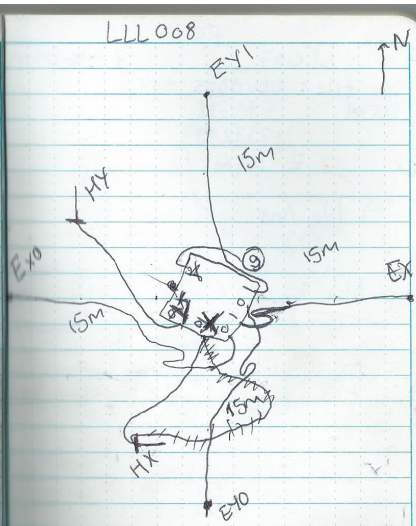

Scale: 1 square = _____

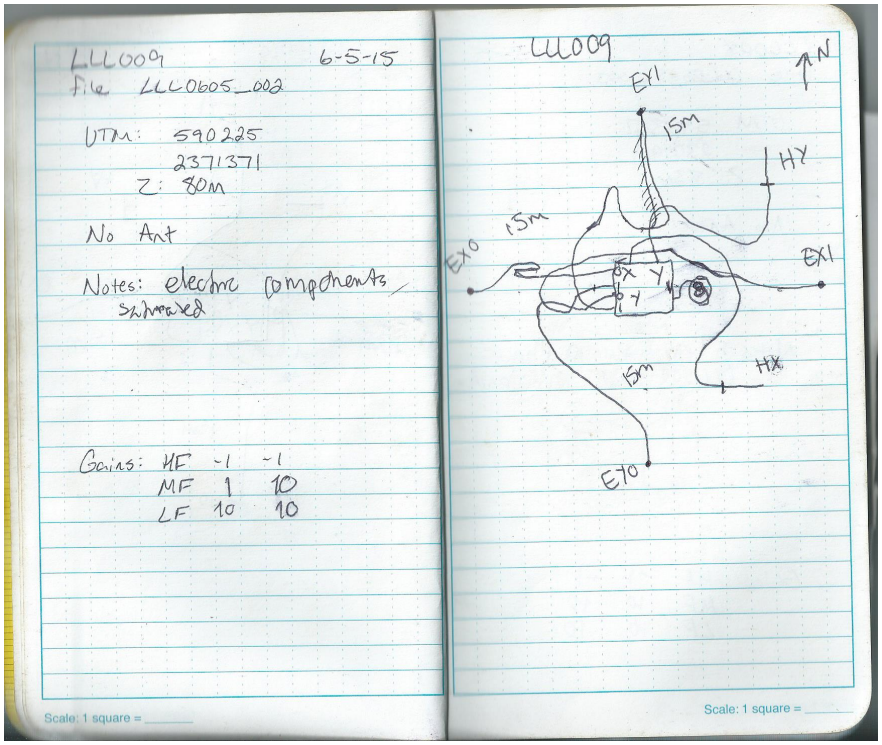

LLL009 6-5-15
file LLL0605_002

UTM: 590225
2371371
Z: 80m

No Ant

Notes: electric components submerged

Gains: HF -1 -1
MF 1 10
LF 10 10

Scale: 1 square = _____

LLL009

N

EX1

15m

HY

15m

EX0

EX1

HX

15m

HX

EY0

Scale: 1 square = _____

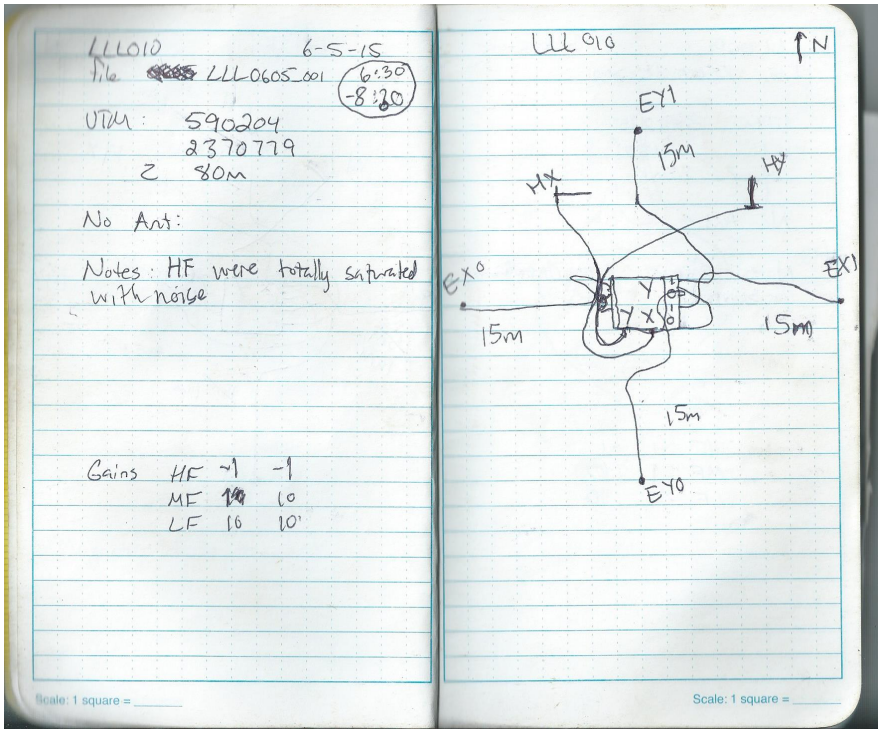

LLL010 6-5-15
file ~~LLL0605_001~~ LLL0605_002 (6:30 -8:30)

UTM: 590204
2370779
Z 80m

No Ant:

Notes: HF were totally saturated with noise

Gains HF -1 -1
MF 1 10
LF 10 10

Scale: 1 square = _____

LLL010

N

EY1

15m

HX

HY

EX0

EX1

15m

15m

15m

EY0

Scale: 1 square = _____

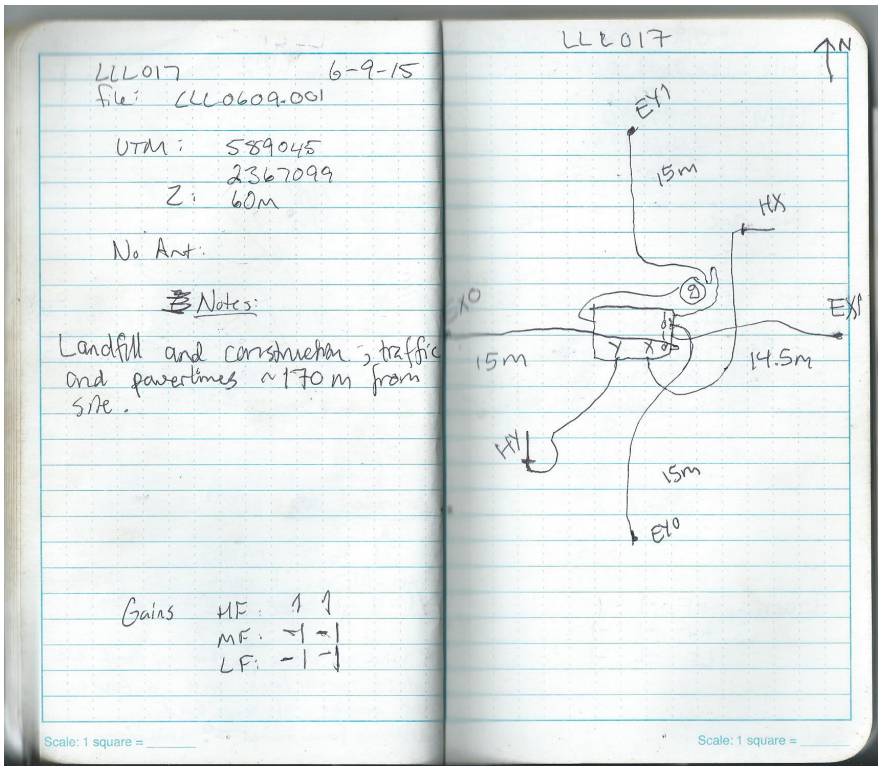

LLL017 6-9-15
file: LLL0609.001

UTM: 589045
2367099
Z: 60m

No Ant:

Notes:

Landfill and construction, traffic and powerlines ~170 m from site.

Gains HF: 1 1
MF: -1 -1
LF: -1 -1

Scale: 1 square = _____

LLL017

N

EY1
15m
HX
EX0
EX1
15m
14.5m
HY1
15m
EY0

Scale: 1 square = _____

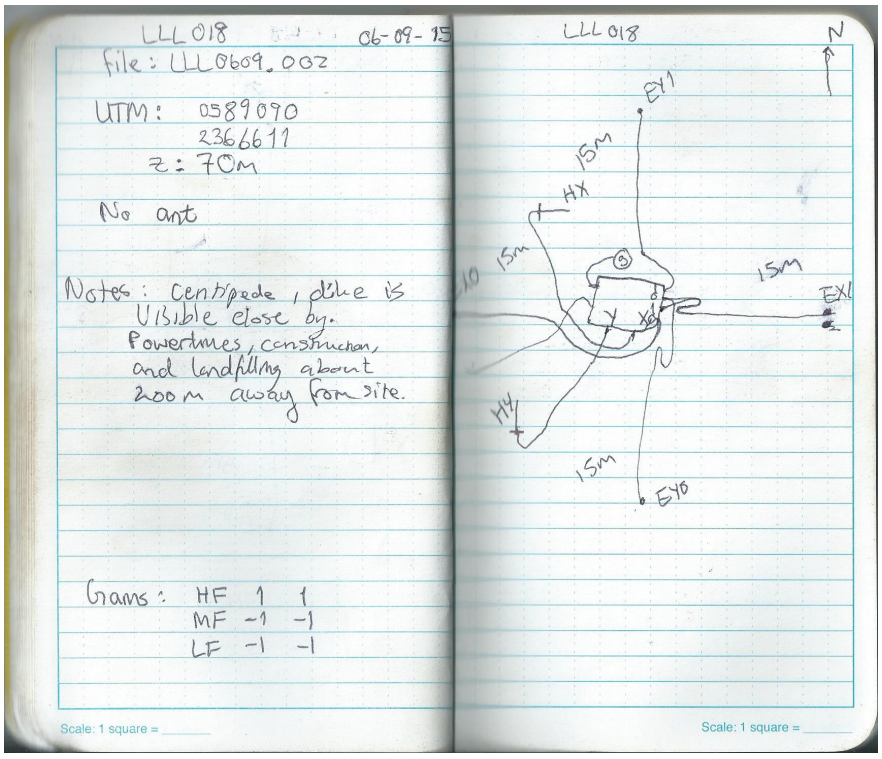

LLL018 06-09-15
file: LLL0609.002

UTM: 0589090
2366611
Z: 70m

No ant

Notes: centipede, dike is visible close by. Powerlines, construction, and landfilling about 200 m away from site.

Grams: HF 1 1
MF -1 -1
LF -1 -1

Scale: 1 square = _____

LLL018

N

EY1
15m
HX
EX0
15m
15m
EX1
HY1
15m
EY0

Scale: 1 square = _____

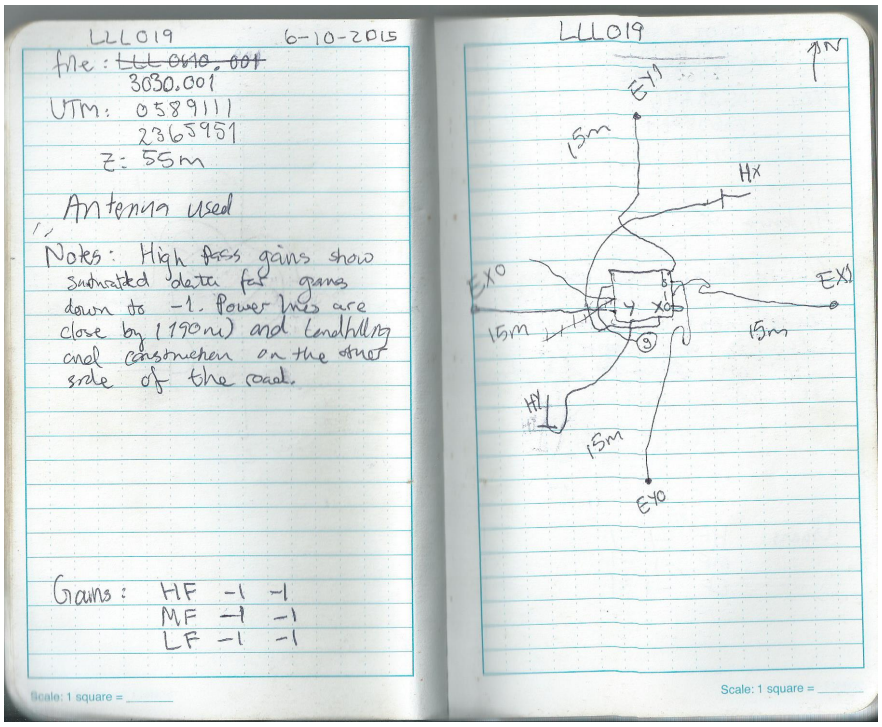

LLL019 6-10-2015

file: ~~LLL0610.001~~
3030.001

UTM: 0589111
2365951

z: 55m

Antenna used

Notes: High ~~freq~~ gains show saturated data for gains down to -1. Power lines are close by (190m) and landfilling and construction on the other side of the road.

Gains: HF -1 -1
MF -1 -1
LF -1 -1

Scale: 1 square = _____

LLL019

Scale: 1 square = _____

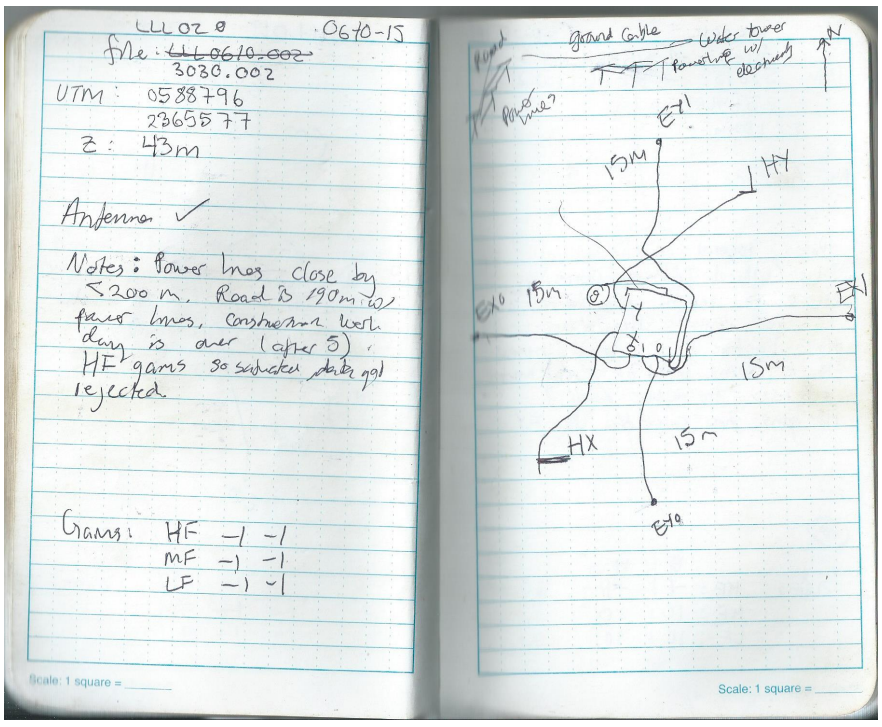

LLL020 06-10-15

file: ~~LLL0610.002~~
3030.002

UTM: 0588796
2365577

z: 43m

Antenna ✓

Notes: Power lines close by ≤200 m. Road is 190m to power lines, construction work day is over (after 5). HF gains so saturated data not rejected.

Gains: HF -1 -1
MF -1 -1
LF -1 -1

Scale: 1 square = _____

Scale: 1 square = _____

B.2 Schofield Barracks

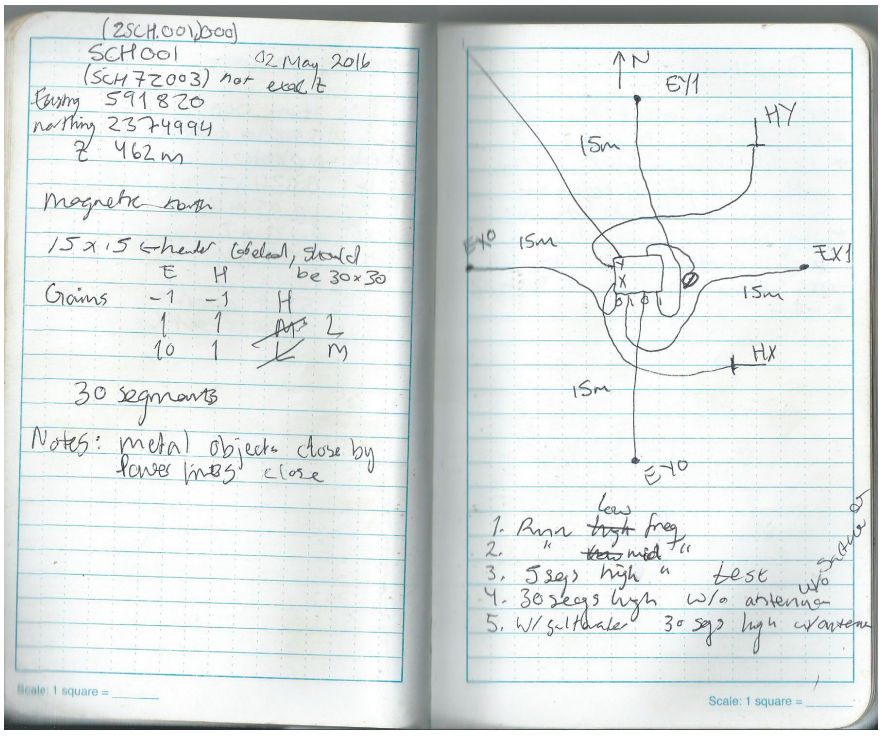

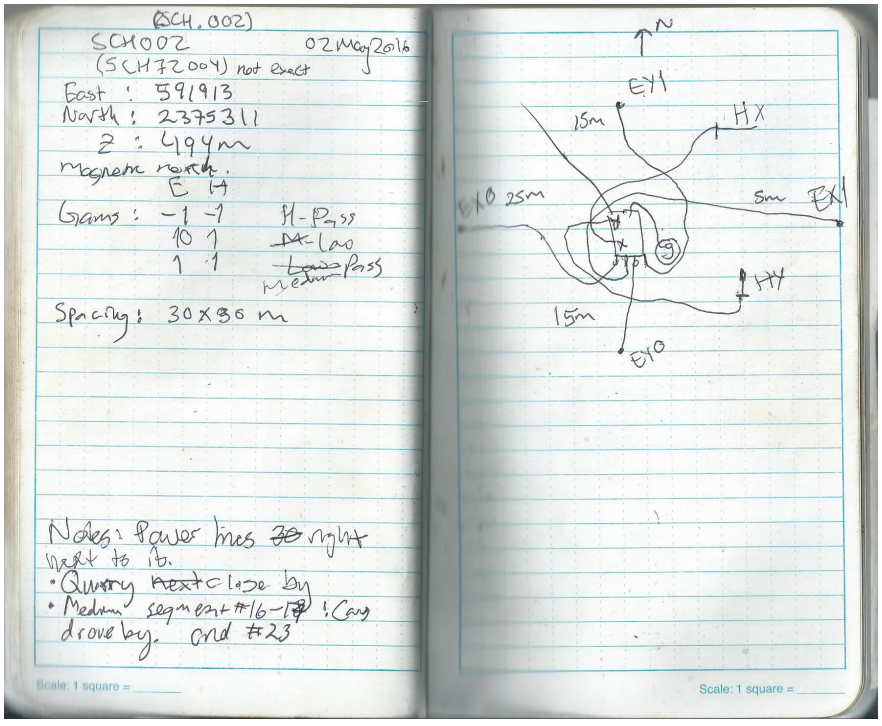

4 May 2016

Live firing on base

SCH003 (SCH72005) not exact
(ZSCH.003)
East: 0592056
North: 2375740
Z: 438m
magnetic declination: -10°
XYZ

	E	H	
Gains:	1	1	High
	~~1~~	-1	~~med~~ low
	1	-1	~~low~~ med

30
Runs: LF: 30 segments
MF: 30 segments
HF: 30 segments

Sketch

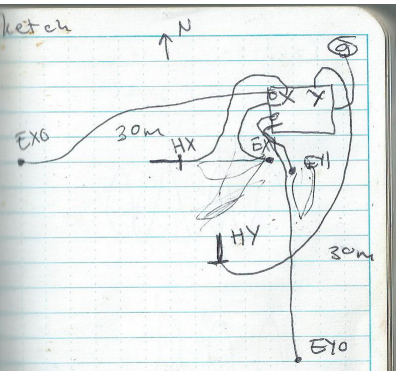

Notes: Bunkers all around live firing. Saw black cute pigs. Saved in the same folder as SCH001 and SCH002
H

Scale: 1 square = _____

Scale: 1 square = _____

4 May '16

SCH004 (" 72006)
(ZSCH.004, 005)
East: 0592267
North: 2376101
Z: 427m
magnetic declination -10°
East-west 24m line
North-south 30m line

	E	H	
Gains:	-1	-1	High-pass
	-1	-1	low-pass
	+1	-1	band pass
			~~med~~

Runs #1: Low FB 30 segs
~~med~~ FB 30 segs
High FB 30 segs

Run #2 Changed Band-pass gains
E = -1 ; H = -1.
low FB 20 segs some skid
mid FB 20 segs
high FB 20 segs

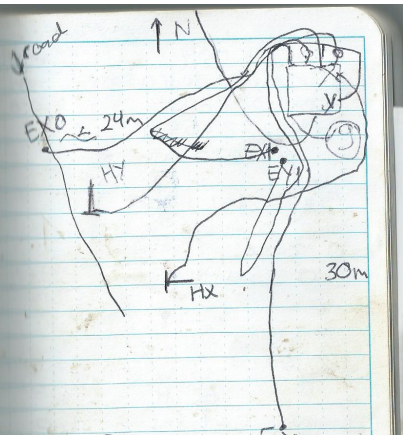

Notes: Powerlines lie parallel over EX line there is another powerline intersecting the other powerline also, more pigs.
Live firing even closer than at the previous sites.

Scale: 1 square = _____

Scale: 1 square = _____

B.3 Waianae Kai

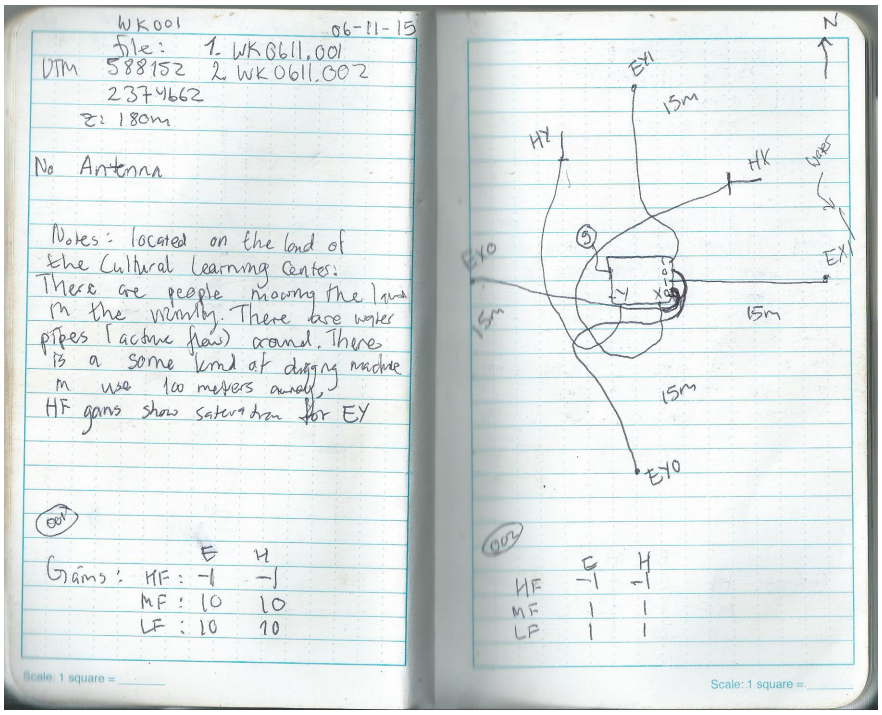

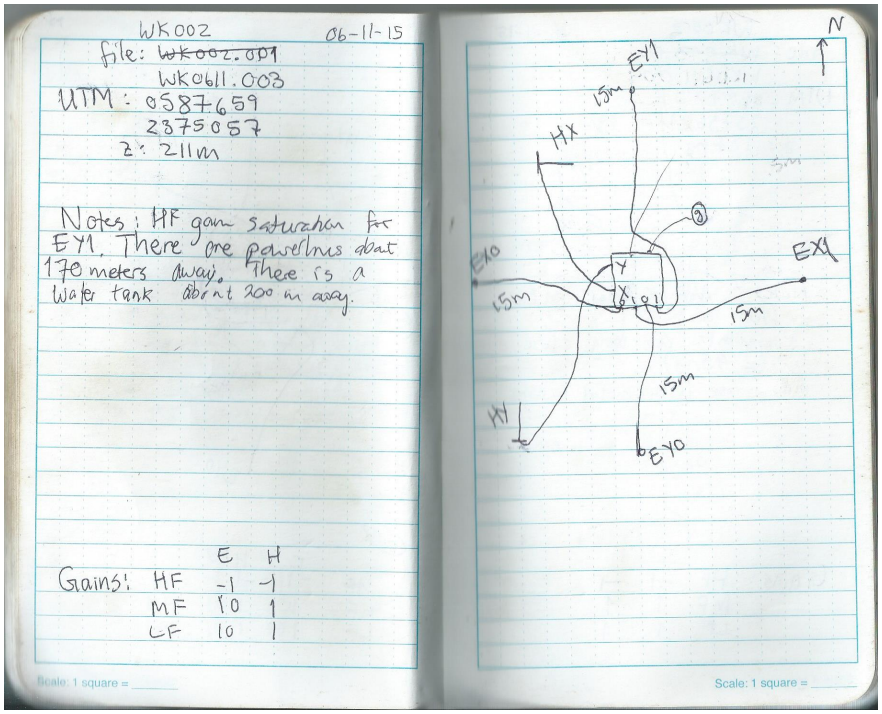

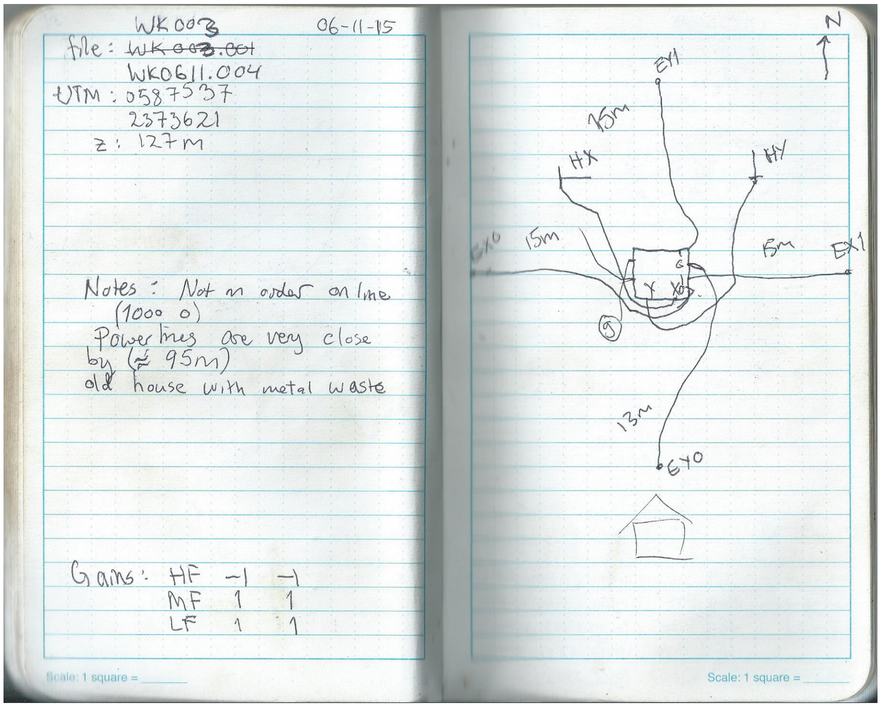
WK003
06-11-15
file: WK0611.004
UTM: 0587537
2373621
z: 127m
Notes: Not in order on line
(1000 0)
Powerlines are very close
by (≈ 95m)
old house with metal waste
Gains: HF -1 -1
MF 1 1
LF 1 1
Scale: 1 square =
N
EY1
15m
HX
HY
EX0
15m
15m
EX1
X
Y
g
13m
EY0
Scale: 1 square =

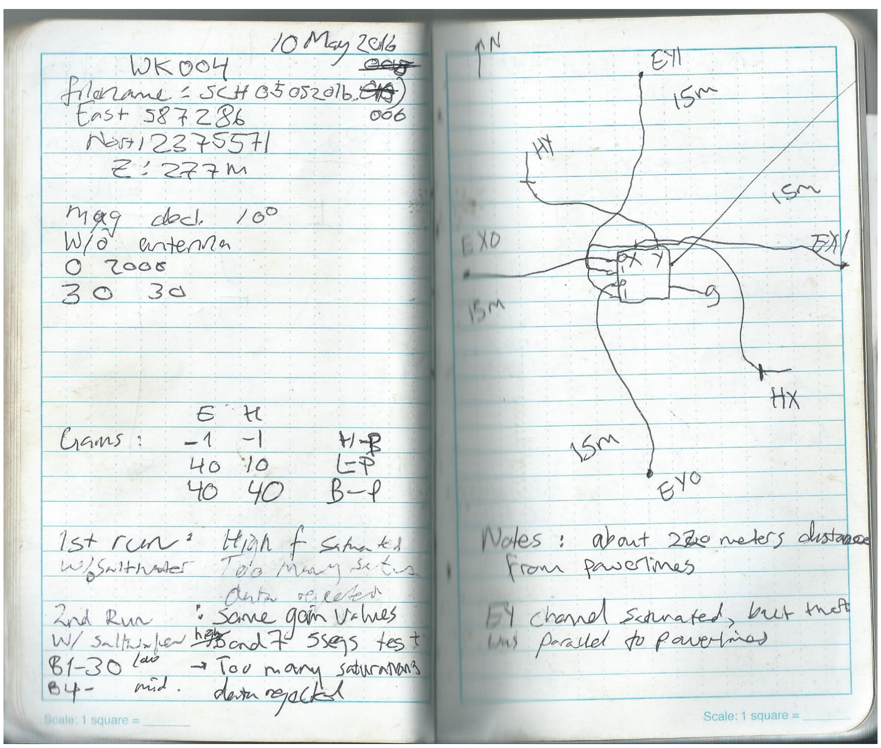
10 May 2016
WK004
filename: SCH05052016.006
East 587286
North 2375571
Z: 277m
mag decl. 10°
W/o antenna
0 2000
30 30
E H
Gains: -1 -1 H-P
40 10 L-P
40 40 B-P
1st run: High f saturated
w/o saltwater Too many saturations
data rejected
2nd Run: Same gain values
W/ saltwater high and 7 5segs test
B1-30 low → Too many saturations
B4- mid. data rejected
Scale: 1 square =
N
EY1
15m
HY
15m
EX0
EX1
X
Y
15m
g
HX
15m
EY0
Notes: about 220 meters distance
from powerlines
EY channel saturated, but that
was parallel to powerlines
Scale: 1 square =

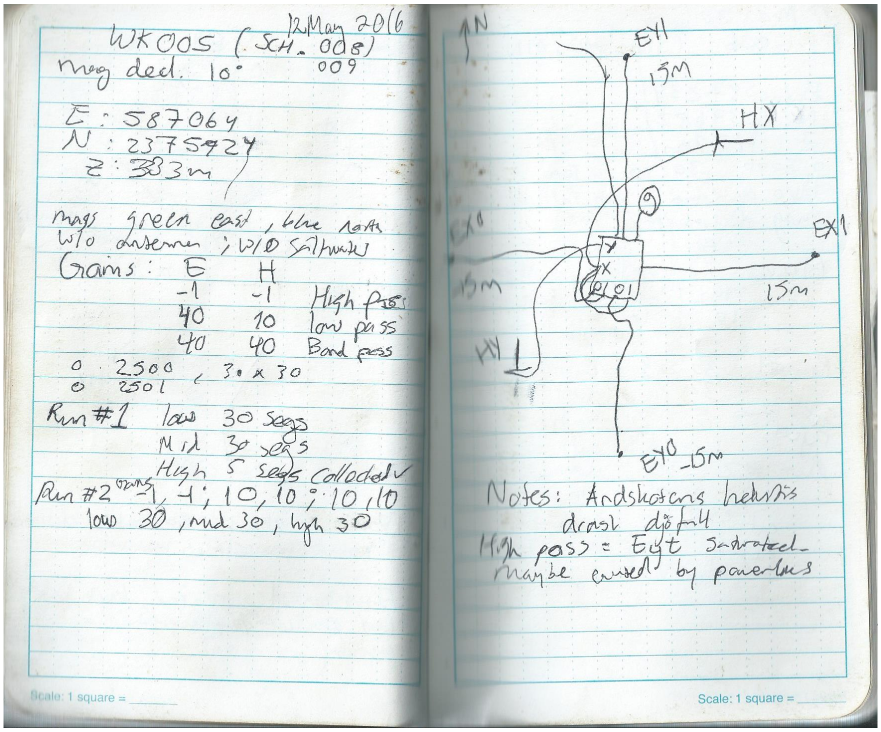

12 May 2016
WK005 (SCH. 008) 009
mag decl. 10°

E: 587064
N: 2375927
Z: 333m

mags green east, blue north
w/o antenna; w/o saltwater

Gains: E H
-1 -1 High pass
40 10 low pass
40 40 Band pass

0 2500, 30 x 30
0 2501

Run #1 low 30 segs
Mid 30 segs
High 5 segs collected ✓
Run #2 gains -1, -1; 10, 10; 10, 10
low 30, mid 30, high 30

Notes: Andskotans helvítis
drasl djöfull
High pass = EY1 saturated
maybe caused by powerlines

Scale: 1 square = ______

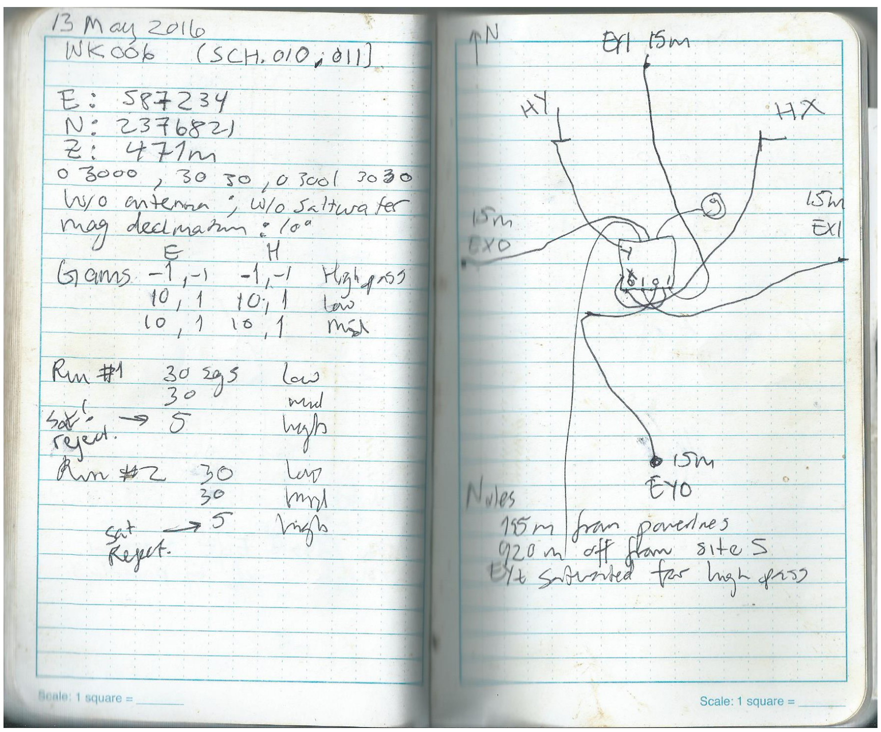

13 May 2016
WK006 (SCH. 010, 011)

E: 587234
N: 2376821
Z: 471m
0 3000, 30 30, 0 3001 3030
w/o antenna; w/o saltwater
mag declination: 10°

	E	H	
Gains	-1, -1	-1, -1	High pass
	10, 1	10, 1	Low
	10, 1	10, 1	Mid

Run #1 30 segs low
30 mid
Sat! reject. → 5 high
Run #2 30 low
30 mid
Sat Reject. → 5 high

Notes
155 m from powerlines
920 m off from site 5
EY1 saturated for high pass

Scale: 1 square = ______

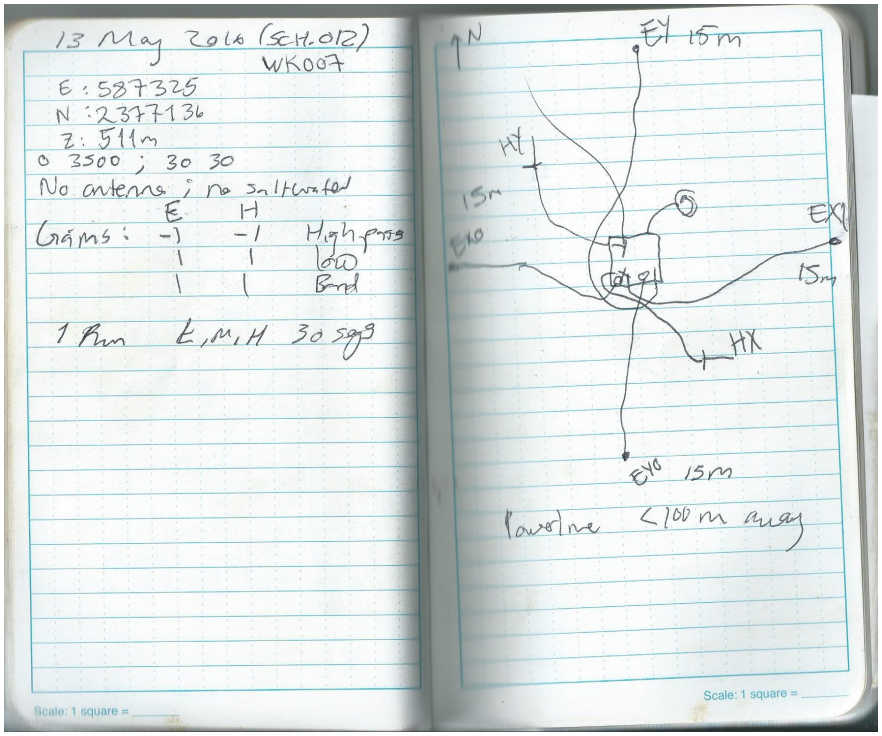

C Successful Permit proposals

In this appendix, accepted documents that were proposed for access permits in Waianae Range, are included.

DAVID Y. IGE
GOVERNOR OF HAWAII

SUZANNE D. CASE
CHAIRPERSON
BOARD OF LAND AND NATURAL RESOURCES
COMMISSION ON WATER RESOURCE MANAGEMENT

KEKOA KALUHIWA
FIRST DEPUTY

JEFFREY T. PEARSON
DEPUTY DIRECTOR - WATER

AQUATIC RESOURCES
BOATING AND OCEAN RECREATION
BUREAU OF CONVEYANCES
COMMISSION ON WATER RESOURCE MANAGEMENT
CONSERVATION AND COASTAL LANDS
CONSERVATION AND RESOURCES ENFORCEMENT
ENGINEERING
FORESTRY AND WILDLIFE
HISTORIC PRESERVATION
KAHOOLAWE ISLAND RESERVE COMMISSION
LAND
STATE PARKS

STATE OF HAWAII
DEPARTMENT OF LAND AND NATURAL RESOURCES

Division of Forestry and Wildlife - Makiki Branch
2135 Makiki Heights Drive
Honolulu, Hawaii 96822

Permit: ODF-082615R

PERMIT FOR ACCESS AND SPECIAL USE

****Permit must be in investigator's possession at all times while on the property.****

PERMISSION IS GRANTED TO: Donald M. Thomas, John Sinton, Cody Winchester, Telma Dis Sigurdardottir and Ikaika Villanueva

FOR THE FOLLOWING PURPOSE: Vehicular access in Waianae Kai FR. Take measurements of the resistivity structure of the subsurface. The purpose of this study is to investigate the geological features of the area such as geochemistry, water table level and the interface of saltwater and freshwater.

LOCATION:

Waianae Kai FR Waianae Kai FR (Restricted Watershed)

FOR THE PERIOD: September 1, 2015 to September 31, 2015

SPECIAL CONDITIONS:

1. All material collected remains under the ownership of the Division of Forestry and Wildlife and may be recovered at any time.
2. This permit does not authorize camping unless otherwise stated.
3. Activities conducted under this permit will be limited to those described in the application dated August 7, 2015 on file with the Division of Forestry and Wildlife office, and hereby made a part of this permit.
4. Copies of any and all preliminary progress reports or publications resulting from this research will be provided to the Hawaii Division of Forestry and Wildlife, Oahu Branch and the Division of Forestry and Wildlife Administration Office in Honolulu. Preliminary report is due December 31, 2015. Final report is due to DOFAW by December 31, 2016.
5. Material collected will not be used for resale.
6. Hiking boots and clothing will be cleaned prior to entry of forest reserve to prevent the spreading of noxious weeds.
7. This permit is not valid unless the signature page is embossed.
8. This permit does not authorize the take of plants or animals Federally listed as Threatened or Endangered as described in the Endangered Species Act of 1973.
9. Open fires and littering are prohibited.
10. Motor vehicles shall be used only on established roadways.

Hawaii Revised Statues (Actions By and Against the State) and Chapter 662, Revised Statues (State Tort Liability Act) for all claims and demands for property damage, loss, personal injury or death caused by the negligent or wrongful act of omission of any officer of employee of the RCUH while acting within the scope of the office of employment, or persons acting for RCUH in an official capacity, temporarily, whither with or without compensation.

Donald M. Thomas
Principal Investigator

APPROVED BY:

David G. Smith
Forestry and Wildlife Manager

8/27/15
Date of Issue

cc: DOCARE

Department of Land and Natural Resources
Division of Forestry and Wildlife
1151 Punchbowl St., Room 325
Honolulu, HI 96813
(808) 587-0063, (808) 587-0064 (Fax)

Application for Research / T&E Collection / Access / Activity Permit

---

Application Date: 8/7/2015

Name and Title of Principal Investigator or Coordinator:
Dr. Donald M. Thomas, Geochemist, Director of Center for the Study of Active Volcanoes

Agency/Organization Supporting Activity:
Funded under two office of Naval Research awards: Aprises 11 Award # N00014-12-1-0496 and Aprises 12 Award #N00014-13-1-0463

Mailing Address:
University of Hawaii
200 W. Kawili
Hilo HI 96720

Telephone Number ~~(808) 956-6482~~ **FAX** (808) 956-3188

E-mail address dthomas@soest.hawaii.edu **Local Contact** ~~Telma Dis Sigurdardottir.~~
Telephone number: (808) 670-7034

Type of Permit(s): NARS__ T&E Species__ Research x Landing__ Access x
Commercial Activity____

Statement of Proposed Activity (Attach study/activity plans and supplementary material as necessary). Audiomagnetotellurics (AMT) measurements in Waianae Kai

1) **How will study/activity results benefit the area, resource, or management in the future?** This study will investigate the subsurface, giving results that can tell us about anomalous resistivity and hence the geological features of the area, such as geochemistry, water table level, and the interface of saltwater and freshwater.

   Study/activity objectives. We will make measurements in the area, using the AMT method. This method enables us to map the resistivity structure of the subsurface. Resistivity is related to conductivity, porosity, and fluid types, enabling us to investigate the geochemistry and conductivity properties of the area.

2) **Specific study/activity location(s). Attach map if needed.**

5) **How is the study/activity to be accomplished? What are the methods to be used? Be specific in listing study/survey techniques and include efforts that will be taken to minimize effects on the resource and/or area.**

We start by laying out four electrodes and two magnetic coils in the study area and connect them to analog front end (AFE) box and that is connected to the Stratagem console, where the data is recorded with. This setup takes up an area of 30 m by 30 m. An electrode is a spike and it is the size of a very large nail. It is about 20 inches long and ¾ inch in diameter. The electrodes are inserted into the ground using a hammer. An example of an electrode is shown in Figure 2.

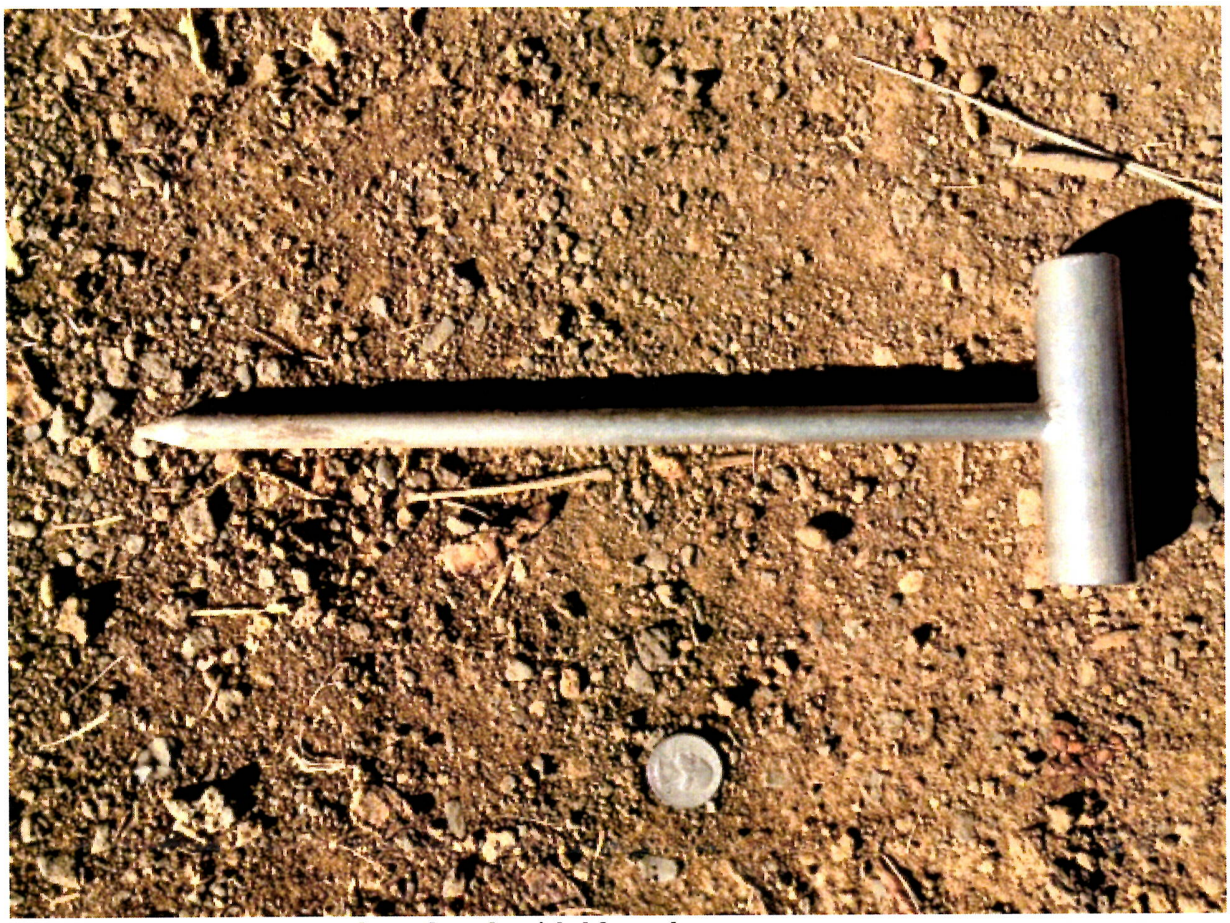

Figure 2: The figure shows an electrode and a nickel for scale.

The two magnetic coils are positioned on top of the ground and oriented precisely to North and to East. Figure 3 shows the equipment for the setup, including the magnetic coils, electrodes, AFE box, the console and all the cables that connects the instrument to the box.

7) **Have any studies (in the case of research proposals) been made that are similar to the one proposed? If yes, please cite.** Yes, Zohdy and Jackson made a study for groundwater exploration on Oahu, their paper was published in 1969. They used deep electrical soundings in their study. Herbert A. Pierce and Donald M. Thomas also investigated groundwater in 2009, using AMT and Magnetotellurics. Their report is cited here as well.

Citation:

Zohdy, A. A. R. & Jackson, D. B. (1969). Application of deep electrical soundings for groundwater exploration in Hawaii. Geophysics, Vol. 34, NO. 4, P. 584-600.

Pierce, H. A. & Thomas, D. M. (2009). Magnetotelluric and Audiomagnetotelluric groundwater survey along the Humu'ula portion of Saddle road near and around the Pohakuloa training area, Hawaii. U.S. Department of the Interior, U.S. Geological Survey, Open-File Report 2009-1135, version 1.1.

8) **Who will participate in the study/activity (in the case of groups, list the leaders and/or responsible parties, or the principal permit holder who will carry overall responsibility)?**

Principal Coordinator: Donald M. Thomas
(As appears on Drivers License)

Title: Geochemist, Director of Center for the Study of Active Volcanoes

Background/Qualifications: PhD Geochemistry. 43 years research on groundwater geochemistry and hydrology of Hawaii.

Assistant: John M. Sinton
(As appears on Drivers License)

Title: Professor (UH Faculty)

Background/Qualifications: PhD geology; 40 years research on Waianae Volcano and Oahu geology.

Assistant: Telma Dis Sigurdardottir
(As appears on Drivers License)

Title: Graduate Student

Background/Qualifications: B.S. Geophysics Studying for MS in Geophysics. 3 summers worth of experience in geophysical surveys in Iceland

Assistant: Cody Winchester
(As appears on Drivers License)

Title: UH employee

Background/Qualifications: B.S. Geology and Geophysics; 3 years experience conducting geophysical surveys in Hawaii

Assistant: Ikaika Villanueva
(As appears on Drivers License)

Title: UH employee

Background/Qualifications: graduate of Kamehameha Schools, an RCUH employee with two years of experience in MT and AMT geophysical surveys

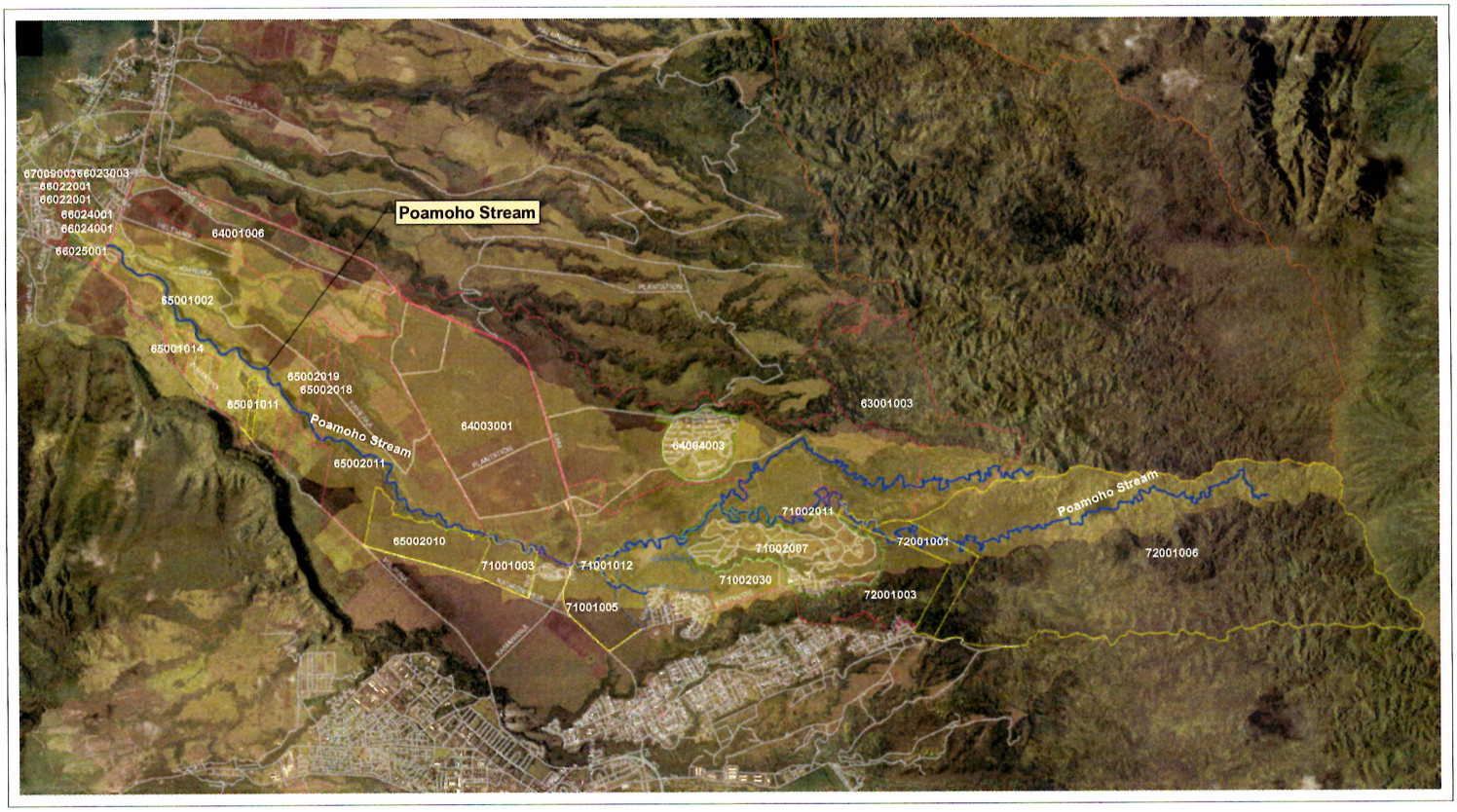

Waialua-Kaiaka Watershed Based Plan
Geomorphology Study Area

D MATLAB scripts

```
function appres
%This function receives MT impedance files and plots apparent resistivity
% and phase with the period.
% August 21st, 2015
%

delete('*.png'); %Delete any images, so that this script can read all the files.
%--------------------------------------------------------------------------
% Definition of variables
%--------------------------------------------------------------------------
S=dir('Z*');
clf
for i=1:length(S)
x{i}=S(i).name;

Z = textread(x{i});%Impedance matrix
n = 2;
f = Z(1:n:end,1); %frequency
T = 1./f; %period
w=2*pi*f; %angular frequency
uo=4*pi*10^-7; %magnetic permeability

rho_xy = Z(1:n:end, 3); %ExHy scalar apparent resistivity
rho_yx = Z(1:n:end, 6); %EyHx scalar apparent resistivity
phs_xy = Z(1:n:end, 4); %ExHy scalar phase
phs_yx = Z(1:n:end, 7); %EyHx scalar phase
co_xy = Z(1:n:end, 2); %ExHy coherency
co_yx = Z(1:n:end, 5); %EyHx coherency

rezxx= Z(2:n:end,1); % re Zxx/sqrt(omega mu_0)
imzxx= Z(2:n:end,2); % im Zxx/sqrt(omega mu_0)
rezxy= Z(2:n:end,3); % re Zxy/sqrt(omega mu_0)
imzxy= Z(2:n:end,4); % im Zxy/sqrt(omega mu_0)
rezyx= Z(2:n:end,5); % re Zyx/sqrt(omega mu_0)
imzyx= Z(2:n:end,6); % im Zyx/sqrt(omega mu_0)
rezyy= Z(2:n:end,7); % re Zyy/sqrt(omega mu_0)
imzyy= Z(2:n:end,8); % im Zyy/sqrt(omega mu_0)

rhocalc_xx = (0.2./f).*((rezxx).^2); %resistivity diagonal elements xx (calculated from rea
rhocalc_yy = (0.2./f).*((rezyy).^2); % resistivity diagonal elements yy (")
rhocalc_xy = (0.2./f).*((rezxy).^2); % resistivity off diagonal elements xy (")
rhocalc_yx = (0.2./f).*((rezyx).^2); % resistivity off diagonal elements (")


tphsxy = atan2(rezxy,imzxy)*180/pi;%ExHy tensor phase
tphsyx = atan2(rezyx,imzyx)*180/pi; %EyHx tensor phase
tphsxx = atan2(rezxx, imzxx)*180/pi; %ExHx tensor phase
tphsyy = atan2(rezyy, imzyy)*180/pi; %EyHy tensor phase
```

```
cxy= complex(rezyx,imzyx); %coherency HyEx
cyx= complex(rezxy,imzxy); %coherency HxEy
resxy = abs(cxy.*cxy); %ExHy tensor apparent resistivity
resyx = abs(cyx.*cyx); %EyHx tensor apparent resistivity

%--------------------------------------------------------------------------
% Plots and figures
%--------------------------------------------------------------------------

appres_loop = figure(i);

subplot(2,1,1) %upper graph is for apparent resistivity from impedance file (containing cor
loglog(f, resxy, 'bs', 'LineWidth',1)
hold on
loglog(f, resyx, 'rs','Linewidth',1)
hold off
xlim([10 100000])
title('Results from site x');
ylabel('Apparent resistivity (Ohm m)');
legend('Rho-xy','Rho-yx')
title(['site ' num2str(x{i})])

subplot(2,1,2) %lower graph is for phase
semilogx(f, tphsxy, 'bs','LineWidth',1)
hold on
semilogx(f, tphsyx, 'rs','LineWidth',1)
hold off

xlabel('Frequency (Hz)');
ylabel('Phase ()');
legend('Phase-xy','Phase-yx')
xlim([10 100000])
ylim([-180 180])


print(appres_loop,'-dpng',[num2str(x{i}),'.png'])%save image as .png file

end

end
```

E AMT data files

All the data files from the exploration will be available on the flash drive, provided with this report. All of the AMT data that were collected are stored on there and are available for further processing.

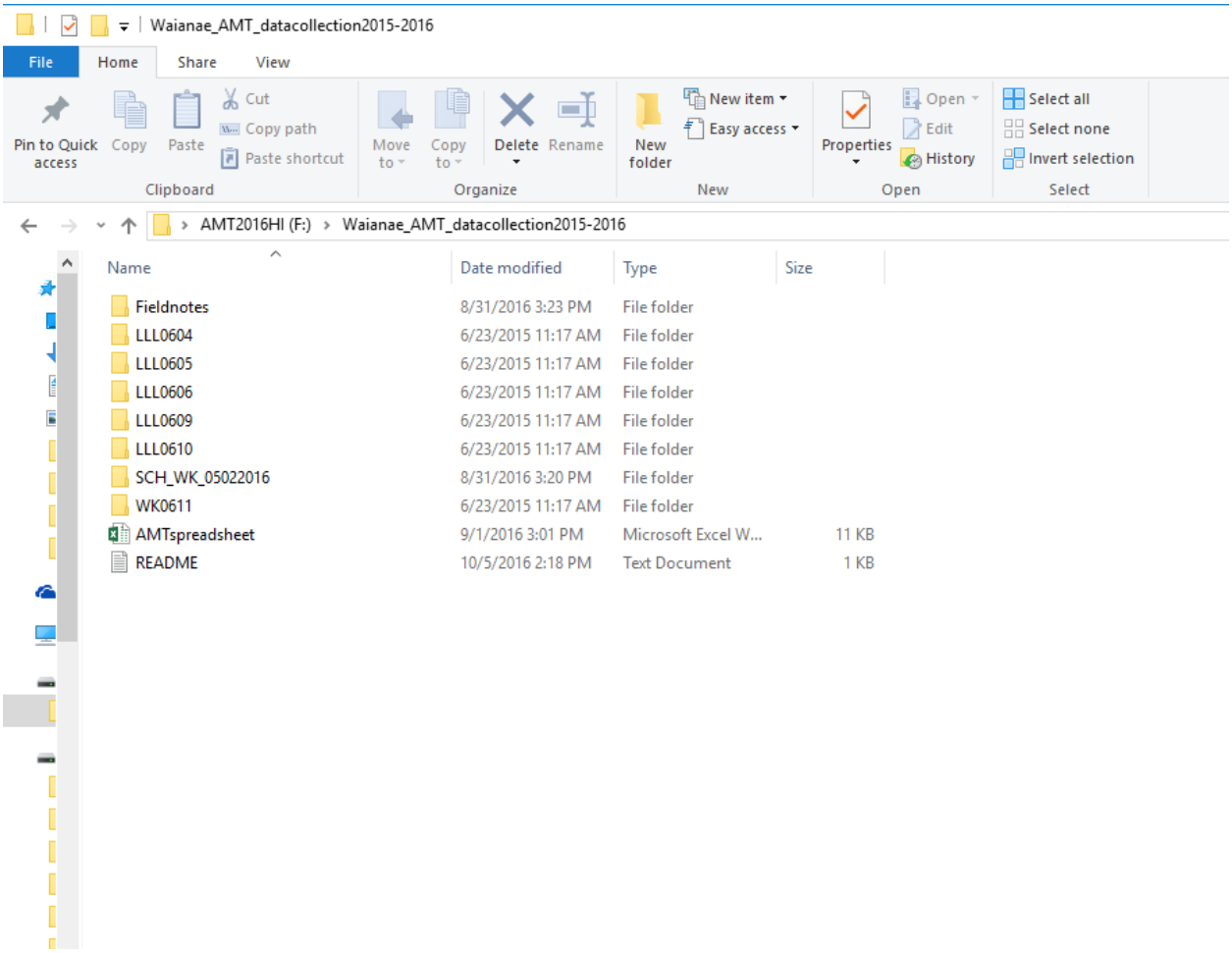

Figure 12: Content stored on a flash drive, available with this report.